DOI:10.1190/1.9781560801924.ch2

Seismic Interferometry without Equations

Simultaneous with the appearance of the GEOPHYSICS supplement on seismic interferometry, THE LEADING EDGE published **Stephen Hill**'s "GEOPHYSICS bright spots" column on seismic interferometry. The author was unfamiliar with the subject at the time he first read the papers in the GEOPHYSICS supplement, but he did a superb job by explaining the principle of seismic interferometry to himself and to the geophysicist for whom this is the first encounter with this new field. The paper by **Andrew Curtis et al.** appeared in the same issue of *TLE* as Stephen Hill's column and gives another clear explanation of the principle of "turning noise into signal" to newcomers, this time written by experts in the field. **Gerard Schuster**'s paper was written for an EAGE workshop and explains the application of seismic interferometry for imaging controlled-source seismic data observed by downhole receivers. He shows that interferometry enables the use of multiple reflections in imaging, which significantly enlarges the illuminated subsurface area. In another *TLE* paper, **Andrey Bakulin** and coauthors discuss the principle of creating a virtual source below a complex overburden by crosscorrelating downgoing and upgoing waves at downhole receivers. The virtual source data obtained in this way are free of overburden distortions, have excellent repeatability, and are therefore well suited for reservoir monitoring. Finally, **Wapenaar and Snieder** discuss the apparent paradox of "turning noise into signal" using an analogy with soccer players, arbiters, and raindrops in a forest. They argue that the robustness of seismic interferometry is explained by the fact that waves have an intrinsic length scale (the wavelength).

GEOPHYSICS bright spots

This special edition of GEOPHYSICS Bright Spots summarizes selected articles from the July-August "Seismic Interferometry" supplement and a single article from a previous issue. Because of the singular focus of the supplement and because this is perhaps a new topic for you, this column is more tutorial than customary.

Virtual source. The creation of a virtual source is a key result of seismic interferometry. If we record traces at two locations from a wide selection of source locations, we can create from the recorded seismic data alone a trace at either of those receiver locations that appears as if the source were at the other location. It is as if we moved a source to one of the receiver locations and thus created a new virtual-source location.

We can do this without knowing the velocity structure of the medium or the locations of the true sources. (Notice that this claim is not the same as the reciprocity theorem, which observes that we can interchange the source and receiver positions and record the same total wavefield as long as there is no directionality at the source or receiver.)

The GEOPHYSICS articles in the supplement on seismic interferometry answer the questions of whether virtual sources work, how to create the virtual-sourced traces, and how to use this method. They also expand on the surprising new field of virtual sources.

In addition to this column, this issue of *TLE* contains a review article, "Seismic interferometry—turning noise into signal," and an article about its application to seismic waves traveling through a building, "Seismic anisotropy of a building."

Motivation first. Starting with the simplest question, "How can virtual sources be used?", consider the determination of the Rayleigh-wave velocity in the near surface of California. In the GEOPHYSICS supplement, Larose et al. use measured wavefields from a grid of California earthquake-monitoring stations (Figure 1) to create new measured wavefields at each receiver location as if each other receiver location were an impulsive source location. With this, Figure 1 becomes a map of receiver locations and virtual-source locations in all possible combinations between sources and receivers.

Figure 2 shows the result of the tomographic Rayleigh-wave velocity inversion, obtained from the synthesized virtual-source observations. These estimated Rayleigh-wave velocities correspond to known significant geologic features. Impressively, with the random noise of the ocean as the energy source, the method produced believable (and not random) results.

The key to creating Figure 2 was the creation of new time series at one receiver location as if a second receiver location were the location of an impulsive source, a virtual source. The authors create the desired time series by cross-correlating the recorded time series for locations A and B, creating a new virtual-source time series as if the source were at A and the receiver at B and, through reciprocity, vice versa.

Seismic interferometry. The creation of virtual sources through crosscorrelation falls within the definition of seismic interferometry. To quote Wapenaar's paper, "Following Schuster (2001), we use the term *seismic interferometry* for the process of generating new seismic responses by crosscorrelating seismic observations at different receiver locations." Now we find out how it works for the creation of virtual sources.

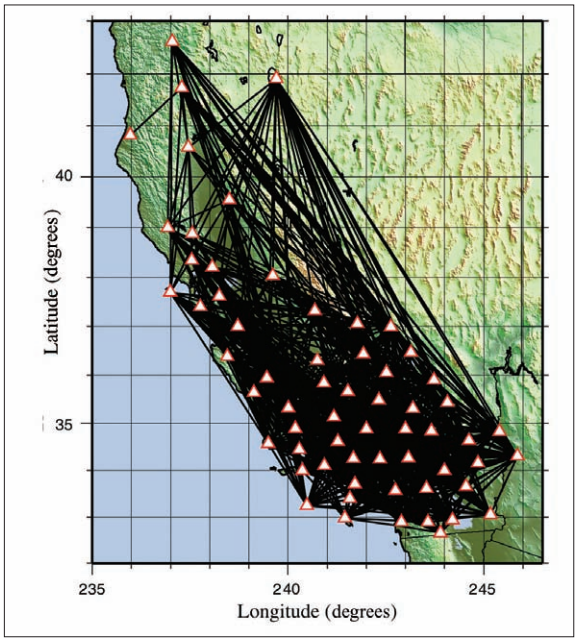

Figure 1. Black lines show possible connecting paths for a California grid of earthquake monitoring stations. (Figure 6, Larose et al., "Correlation of random wavefields: An interdisciplinary review.")

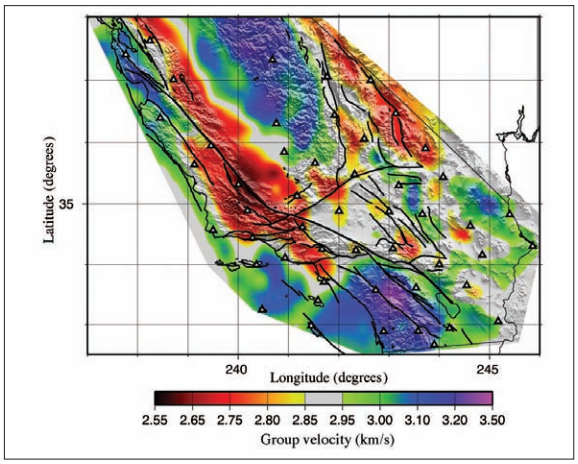

Figure 2. Rayleigh-wave group velocity obtained from tomographic inversion. (Figure 7, Larose et al., "Correlation of random wavefields: An interdisciplinary review.")

Huygens' principle. Using the geometry shown in the upper part of Figure 3, van Wijk simultaneously measured wavefields at two locations (x and x') on a granite slab in the laboratory. The solid raypaths contribute to the observations at both x and x'. The dotted raypath represents paths that contribute only to the observations at x. Using Huygens' principle, each location acts like a new source. Thus, we may

Reprinted from THE LEADING EDGE, **25**, 1078–1081.

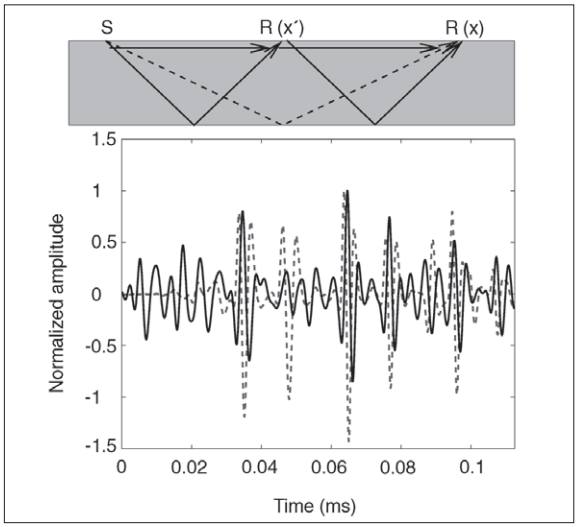

Figure 3. Laboratory configuration (top) and comparison of recorded wave with source at x′, receiver at x (dotted line), and crosscorrelation of recorded waves with source to left of receivers at x′ and x. (Figure 3, van Wijk, "On estimating the impulse response between receivers in a controlled ultrasonic experiment.")

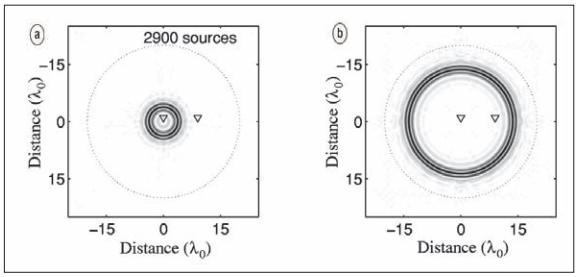

Figure 4. Wavefield synthesized through crosscorrelation technique. The outer ring of light dots represents the lateral locations of the ring of sources. (Figure 1, Larose et al., "Correlation of random wavefields: An interdisciplinary review.")

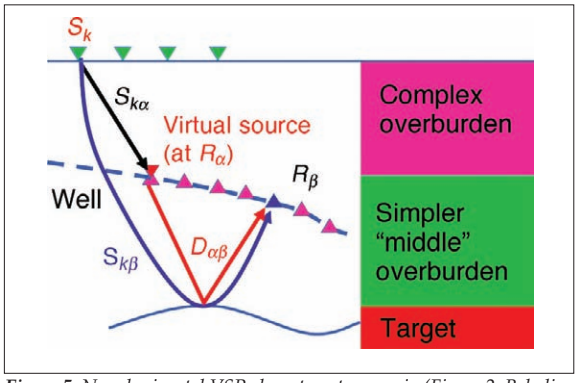

Figure 5. Near-horizontal VSP above target reservoir. (Figure 2, Bakulin and Calvert, "The virtual source method: Theory and case study.")

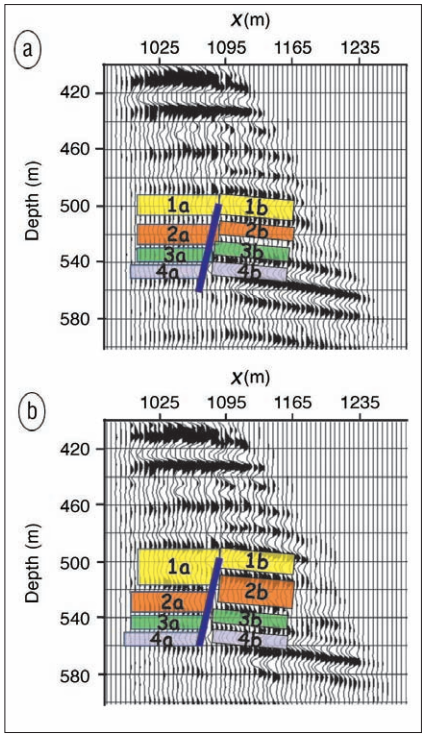

Figure 6. Time-lapse comparison of reservoir images obtained by migrating virtual-source VSP data. Baseline survey (top) and monitor survey (bottom). (Figure 19, Bakulin and Calvert, "The virtual source method: Theory and case study.")

view the measured wavefield at x' as the source for the solid raypaths recorded at location x.

Similar to a vibroseis correlation, van Wijk correlates the seismic data recorded at x' with that recorded at x to remove the Huygens' wavelet source signature at x'. He shows the result of crosscorrelation as the solid curve in Figure 3. That crosscorrelation is the virtual-source trace.

For comparison, the dotted curve is the trace obtained from a laboratory measurement with a source at x' and the receiver at x. We will call that curve the $S(x')$ trace. The curves are not identical (normalized crosscorrelation coefficient equals 0.65) because there are rays from S to $R(x)$ that were not recorded by $R(x')$. The author expands the experiment by placing an additional 39 sources in a line, all to the left of the two receiver locations.

The author then sums (stacks) the individual crosscorrelations between $R(x)$ and $R(x')$ obtained from the 40 virtual-source traces, obtaining an improved virtual-source trace. This summation emphasizes the contributions of the raypaths seen by both $R(x')$ and $R(x)$, increasing the normalized crosscorrelation between the improved virtual-source trace and the $S(x')$ trace to 0.87. Thus, the summation of the crosscorrelations of the traces obtained at $R(x')$ and $R(x)$ is almost identical (crosscorrelation coefficient equals 0.87) to the trace with a source at x' measured by $R(x)$. The crosscorrelation technique creates a virtual source at x', assuming that the wavefield recorded at x', through Huygens' principle, provides the source signature at x'.

Notice that in apparently moving the source from its true location to create a virtual source at location x', van Wijk did not have to know the velocity of the medium. The required velocity information is encoded in the two recorded traces, at locations $R(x)$ and $R(x')$. For the same reason, the author did not have to know the locations of the true sources.

Although this example contained only two isolated reflectors (top and base of granite slab), the method requires no information about reflector locations or characteristics.

Virtual-source test. To test the ability to create virtual-source traces, Larose et al. first create a 2D wave-equation model.

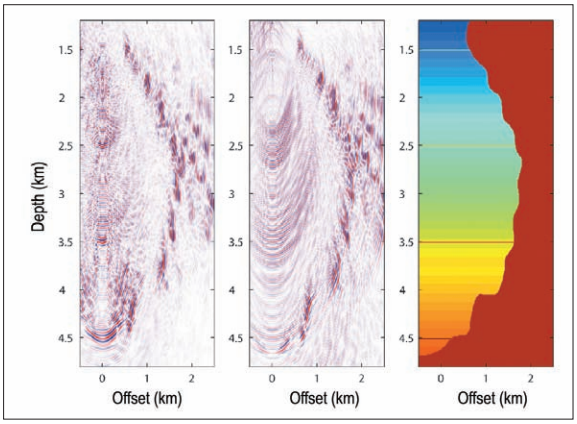

Figure 7. *Salt-face images produced from model downhole data: left, from downhole source and receiver model data; center, from surface-source, downhole receiver model data converted to virtual-source data; right, velocity model of salt wall. (Figure 4, Willis et al., "A novel application of time-reversed acoustics: Salt-dome flank imaging using walkaway VSP surveys.")*

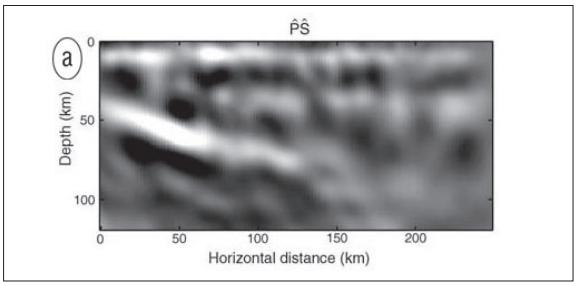

Figure 8. *P-S image of plate subducting beneath Oregon. (Figure 8a, Shragge et al., "Teleseismic shot-profile migration.")*

A ring of sources surrounds a central receiver line. For each independent source location, the authors measure the wavefield at numerous locations within the ring of possible source locations. To create wavefield measurements for a single virtual source at the model's center, the authors summed the crosscorrelations of each trace and the trace recorded at that central location. For this central source, the *x-y-t* volume of the crosscorrelations should reveal a cone-shaped event.

In Figure 4, we see this cone in two time slices, demonstrating that the volume of crosscorrelations properly recreates a central source, using only data obtained from a cylinder of source locations. Larose et al. go beyond verification of the virtual-source method by investigating its robustness for data obtained from a partial ring of sources. If the medium contains a uniformly random distribution of scatters, the scatterers act as new sources, providing a full-angle illumination allowing for an accurate reconstruction of data for a central virtual source. Minus the scatterers, the authors obtain only a partial reconstruction.

Improved reservoir monitoring. This example and others to follow further demonstrate that sources need not surround receivers to provide adequate virtual-source data. Bakulin and Calvert use the VSP geometry shown in Figure 5. Through the virtual-source method, they obtain a clearer image of the differential compaction of the reservoir across a fault (Figure 6) with a virtual source at the well location, avoiding the complex raypaths from the surface to that well. Unlike moving the source from the surface to the wellbore

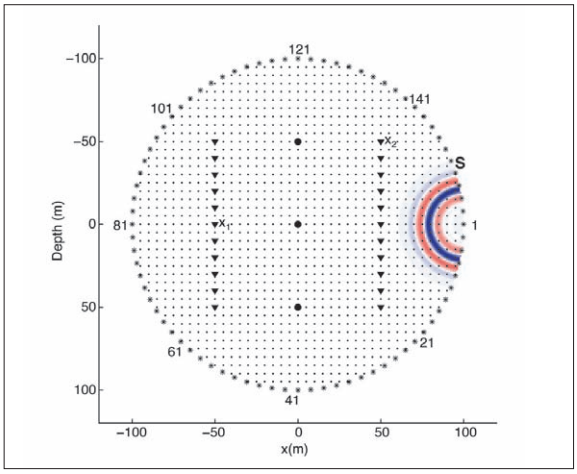

Figure 9. *Recorded impulse source in a homogeneous model. The small filled circles are point scatterers. (Figure 2, van Manen et al., "Interferometric modeling of wave propagation in inhomogeneous elastic media using time reversal and reciprocity.")*

with downward continuation, the virtual-source method (crosscorrelating traces from receiver pairs) allows for source relocation without knowledge of the complex overburden.

As demonstrated in a related article by Korneev and Bakulin (GEOPHYSICS, May-June 2006), we can think of this virtual-source method as redatuming the data to a location beneath the complex overburden by using experimentally measured information, in contrast to the traditional redatuming method that necessarily uses a coarser velocity model.

The additional resolution gained from migration of Bakulin and Calvert's virtual-source VSP data (Figure 6) reveals production-related differential compaction across the fault.

Imaging salt edge. Through VSP data, the virtual-source method is also useful for imaging a nearly vertical salt wall. Assume that we could obtain zero-offset data from a borehole in close proximity to the vertical salt face. This zero-offset data could be depth-migrated, creating an image of the salt face. As reproduced from Willis et al. (GEOPHYSICS, March-April 2006), the left-hand illustration in Figure 7 illustrates the result of this procedure applied to model data.

In contrast to the above geometry, we customarily place sources on the surface and receivers in the hole, which is the geometry of walkaway VSP. To obtain data as if the source were coincident with a downhole receiver, Willis et al. autocorrelate the VSP downhole traces for each surface source location and then sum (stack) the autocorrelations corresponding to a single subsurface receiver position but from different surface source positions. The authors use autocorrelations instead of crosscorrelations because their desired virtual-source locations are coincident with receiver locations.

This technique moves the surface source locations to the downhole virtual-source locations without knowledge of the velocity or the original source-to-receiver separation distance. The recorded first arrival at the downhole location contains the needed time-advance information. Thus, distance and velocity information are not needed.

Now for the results. Willis et al. create the central image of Figure 7 by depth-migrating the zero-offset data obtained through the autocorrelation-based virtual-source method.

Note the similarity of this image to that shown on the left.

In the July-August GEOPHYSICS supplement, Shragge et al. depth-migrate transmission data. The sources are discrete teleseismic events used to create images of the lithospheric structure. These independently distinguishable, distant-triggered events start their upward path in the lower to middle mantle. The reflections from the earth surface act as a new downward-traveling plane-wave source, which then mode-converts and reflects upward as shear waves.

Shragge et al. use the first arrival as the source in their depth migration and the later arrival as transmission/reflection events. From this, along with appropriate velocity structure, the authors image the Juan de Fuca Plate subducting underneath central Oregon (Figure 8).

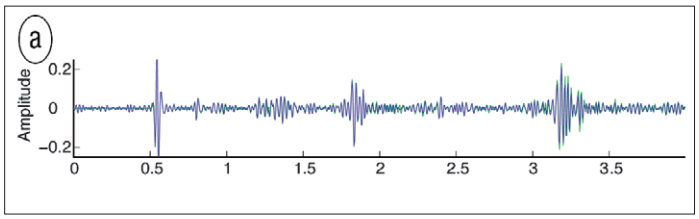

Figure 10. *Comparison of seismic traces obtained from virtual source (blue) and real source (green) at the same locations in the model. (Figure 8, van Manen et al., "Interferometric modeling of wave propagation in inhomogeneous elastic media using time reversal and reciprocity.")*

Interferometric modeling. Van Manen et al. apply interferometry to create arbitrarily sourced wavefield models. As an initial step, the authors obtain a series of model traces from receivers uniformly spaced throughout the model and a single source at the periphery of the model. Figure 9 shows an instant in a recorded wavefield in a homogeneous model that contains three point scatterers. The authors repeat this numerical experiment for each source position along the perimeter of the model. The successive source locations along the circle completely enclose the model. (Any shaped enclosure will work.)

As the second step, van Manen et al. use interferometry to create wavefields as if the source were at any location inside the circle of true sources. As is the case with the previously reported virtual-source applications, the authors generate the desired wavefields through a summation of crosscorrelations. Thus, from a series of shots around the periphery of the model, the authors construct new model traces as if there were an impulsive source at any interior location.

The collection of peripherally shot models provides a complete set of model responses and, from that, the potential to fabricate any new responses through linear superposition of those individually weighted and time-shifted models. The crosscorrelation process provides the weighting and time-shifting. The overlap of the two traces shown in Figure 10 demonstrates the success of this method in recreating a specific trace for the complex 2D elastic Pluto salt model. Because many inversion algorithms contain a modeling step, van Manen et al. suggest that their reported technique holds great promise for such inversions. TLE

—STEPHEN J. HILL
Colorado School of Mines, Golden, USA

Seismic interferometry—turning noise into signal

Andrew Curtis, University of Edinburgh, UK
Peter Gerstoft, University of California at San Diego, USA
Haruo Sato, Tokoku University, Japan
Roel Snieder, Colorado School of Mines, USA
Kees Wapenaar, Delft University of Technology, The Netherlands

Turning noise into useful data—every geophysicist's dream? And now it seems possible. The field of seismic interferometry has at its foundation a shift in the way we think about the parts of the signal that are currently filtered out of most analyses—complicated seismic codas (the multiply scattered parts of seismic waveforms) and background noise (whatever is recorded when no identifiable active source is emitting, and which is superimposed on all recorded data). Those parts of seismograms consist of waves that reflect and refract around exactly the same subsurface heterogeneities as waves excited by active sources. The key to the rapid emergence of this field of research is our new understanding of how to unravel that subsurface information from these relatively complex-looking waveforms. And the answer turned out to be rather simple. This article explains the operation of seismic interferometry and provides a few examples of its application.

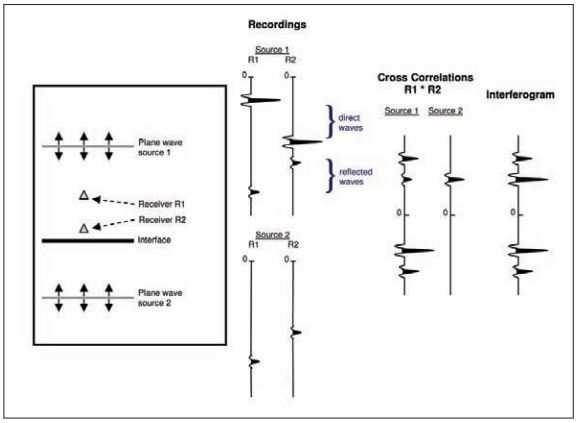

Figure 1. *Interferometric construction of a virtual source. (left) One-dimensional acoustic medium consisting of single interface between two half-spaces, with two plane-wave sources and two receivers. (center) Traces recorded at each receiver for each source. (right) crosscorrelations between pair of traces for source 1 and for source 2, and the sum of these crosscorrelations. At positive times, the final summed trace turns out to be the trace that would be recorded at one receiver if the other had been a source. (Note that the virtual source wavelet in the three traces on the right should in fact be the autocorrelation of the recorded source wavelet shown in the center; we have omitted this change in source wavelet in the figure for simplicity.)*

A simple thought experiment. Consider an example of a horizontally stratified (one-dimensional) acoustic medium, and for the moment let us imagine that it has only a single internal interface. Now, say horizontally planar pressure waves are emitted by two impulsive sources, one after the other, and that one source is above the interface and one below. Vibrations from the resulting propagating waves are recorded at two receivers which can be placed anywhere between the two sources (Figure 1, left).

The recordings are shown in the center of the figure. At each receiver a direct and a reflected wave is recorded for source 1, whereas only one transmitted wave is recorded for source 2.

Seismic interferometry of these data involves only two simple steps: The two recorded signals from each source are crosscorrelated and the resulting crosscorrelograms are summed (stacked). The result, shown on the right of Figure 1, is surprising; for positive times it is the seismogram that would have been recorded at either receiver if the other receiver had in fact been a *source*, and at negative times it is the time reverse of this seismogram. In other words, by this simple, two-step operation we have constructed the seismic trace from a virtual source—a source that did not exist in our initial experiment, and a source that is imagined to be at the location of one of our receivers.

To generalize, this simple example placed no constraint on where the receivers were placed, provided they were between the sources. By moving either or both of them (or by using many distributed receivers from the start), it is therefore possible to construct the trace from an infinite number of virtual source and receiver pairs placed at any locations, by recording the signal from only two actual sources. What is more, provided one of the active sources is above the interface and receivers and the other is below, the location of the active sources is also arbitrary, and in order to carry out the process above we do not even need to know where these sources are.

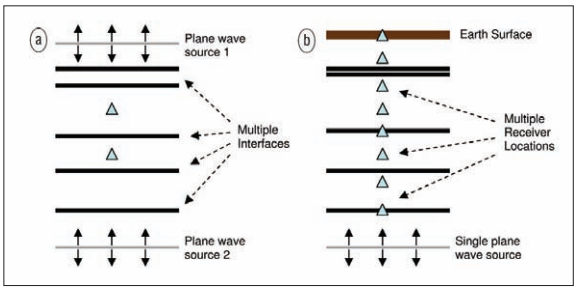

Figure 2. *Alternative, more Earth-like models for which the process in Figure 1 works equally well. (left) Multiple layers with no free surface—still two sources required. (right) Multiple layers with a free surface—only one source required. The right plot also shows that any receiver locations can be used for the virtual source and receiver reconstruction.*

Seismic interferometry steps. The fundamental steps of the operation are simple: crosscorrelation (we can understand this operation as detecting the traveltime difference of the recorded waves between the pair of receivers), then stacking (i.e., integration over all actual sources; a few details required to get the dynamics correct have been omitted for clarity). Yet, the technique is powerful and so far we have barely scratched the surface.

The result above holds for any horizontally stratified medium, still using only two actual sources (Figure 2a). The important criterion for the distribution of actual sources is that they completely surround the medium of interest (a portion of a one-dimensional medium is "surrounded" by two

Reprinted from The Leading Edge, **25**, 1082–1092.

points, at the top and at the bottom). However, if any part of the boundary is a surface of total reflection (like the free surface of the Earth), it turns out that no source is required on that boundary. Hence, in 1D Earth-like models, only a single actual source is required to construct seismic traces between *any* source-receiver pair, including sources or receivers placed on the free surface (Figure 2b). Now, consider a case in which a complex, multilayered medium is situated below the region of the model of interest (between the sources in Figure 2a); this is probably realistic for the Earth. In that case, if source 2 is moved below this complex part of the medium, its contribution to the received signals becomes virtually zero due to transmission losses. In that case, the lower source in Figure 2a can be neglected and again only a single active source is necessary to construct the inter-receiver seismic traces.

The above example also shows us how to make sense of noise and codas (the long, multiply reflected tails of data observed on seismic traces). It turns out that impulsive sources on the boundary can be replaced by uncorrelated noise sources that emit continually and simultaneously. Any pair of extensive noise records from any two receivers can then be crosscorrelated and, remarkably, the result will be approximately the same as above: The crosscorrelation will approximate the impulse response (the measured wavefield at one location if an impulsive source is placed at the location of the other) on the right of Figure 1, convolved with a source time function that is the autocorrelation of the noise. In fact, the first ever seismic interferometry theory, derived by Claerbout in 1968, was for the emergence of the reflection response in cases like Figure 2b where both receivers are placed on the surface and the actual source below (e.g., microseismic activity) emitted random noise.

Generalizing to 3D. What is even more remarkable about the current theory is that with a little modification it is applicable to waves propagating through any lossless (nonattenuating) one-, two-, or three-dimensional medium, and some empirical applications in attenuating media have also been successful (see below). Hence it can also be applied to three-dimensional elastic Earth models. Other than some numerical adjustments, the main modification is that the sources must surround the medium entirely; the stacking or integration step is then performed over the crosscorrelograms from that entire set of sources.

Notice something important about the 1D results: all of the information we need to calculate wave propagation from any source location within the medium is contained within the waves propagating from a single source on the lower boundary in Figure 2b (or from a single source in Figure 2a if the medium is complex outside of the part depicted, as discussed earlier). To record data from multiple sources in a 1D medium is to store redundant data. As the theory generalizes to multiple dimensions, so also does this result: storing data from sources on the boundary of a medium is sufficient to construct data from any other source placed within the medium or on the free surface.

Requirements of 3D seismic interferometry. It is worth noting the main assumptions behind seismic interferometry theory which currently impose limitations on its domain of applicability. First, for an exact application using noise sources on the bounding surface, the medium must be lossless (nonattenuating). Second, if random noise sources (e.g., sources of background noise in the Earth) are to be used in two or three dimensions, then the distribution of that noise must be "even" in senses to be made clear later. Third, as we stated above, if active sources are used, then to obtain dynamically correct responses (i.e., with the correct amplitudes) the sources must completely surround the portion of the medium of interest (other than along completely reflecting boundaries). On this last point, notice that the only place that we do not require sources to completely surround the medium is precisely where physical and cost constraints force us to put them—on the Earth's surface!

Definition of seismic interferometry. The term *interferometry* generally refers to the study of interference phenomena between pairs of signals in order to obtain information from the differences between them. Seismic interferometry simply refers to the study of interference of seismic-related signals. The principal mathematical operation used to study this interference is crosscorrelation of pairs of signals, but one could equivalently consider convolution as the principal operation because crosscorrelation is simply convolution with the reverse of one of the two signals. The signals themselves may come from background-propagating waves or reverberations in the Earth, from earthquakes, from active artificial seismic sources, from laboratory sources, or from waveforms modeled on a computer—examples of using all of these data types will be given below.

The above definition is fairly general and covers a multitude of different "types" of interferometry. For instance, one example presented below uses the crosscorrelation of only two signals recorded at a single receiver from pairs of repeated artificial seismic sources to obtain information about the difference in average seismic velocity of the crust before and after an earthquake occurred. Another example integrates a suite of crosscorrelations of synthetic signals from sources that span the entire boundary of a medium of interest in order to efficiently model waveforms between any sources and receivers contained in the interior of that medium. In each example, various different subsequent processing steps are applied to the data in order to obtain different types of information, but the fundamental initial operation is the same: crosscorrelation.

The majority of different theories and applications using seismic interferometry can be divided into two distinct classes of techniques: those that are predominantly used to obtain information about the medium through which waves have propagated, and those that reconstruct information about the propagated waves themselves. As we will see, each has tangible relevance to the industrial seismic community.

The rise of seismic interferometry into mainstream geophysics has been fueled by a rapid sequence of advances. The majority of the most significant advances have been reported outside of the exploration literature. We will review these important pieces of work (many of which are listed in the appendix) and then show some recent, exciting examples of how this new theory can be applied. The examples include the evaluation of building responses to seismic waves, tomography for crustal properties, changes in crustal properties over time, ground-roll removal from seismic data, and waveform modeling. Finally, we discuss some key challenges for this field in the future.

Historical development of interferometry. The development of what we now think of as interferometry has occurred through several distinct breakthroughs, each of which changed our understanding of how interferometry works. We now review these as they form the fundamental literature behind the supplement to the July-August issue of GEOPHYSICS.

The extraction of the impulse response of a system from

DOI:10.1190/1.9781560801924.ch2

noise is known in physics as the *fluctuation dissipation theorem* (e.g., Callen and Welton, 1951). A system near equilibrium behaves in the same way to an external force as it does to fluctuations within the system (noise); it relaxes to the equilibrium state. However, the birth of interferometry in *seismic* applications can be clearly identified in a paper by Jon Claerbout (1968). He showed that if a 1D medium is bounded on top by a free surface (like the surface of the Earth) and is bounded below by a half-space (homogeneous, infinitely extensive Earth), then the plane-wave reflection response of a horizontally layered medium (what we would record at the surface of the Earth given a source also at the surface) can be obtained from the plane-wave transmission response of the same medium (what we would record if instead the source was in the half-space below). Indeed, he showed that the reflection response is obtained directly by autocorrelation of the transmission response—crosscorrelation of the transmission response with itself. When the source in the half-space below is a noise source, the source wavelet of the reconstructed reflection response is the autocorrelation of the noise.

Claerbout's conjecture. This in itself was of great theoretical interest, but Claerbout also made a phenomenal conjecture: that the crosscorrelation of noise traces recorded at two different receiver locations in three-dimensional, heterogeneous media gives the response that would be observed at one of the locations if there was a source at the other. In other words, simply by listening to noise at two receivers, we can construct the signal that would have been observed if we had used a source at one of the receiver locations. This method to construct artificial seismic sources was to be demonstrated and proven years later (e.g., Rickett and Claerbout demonstrated its application to helioseismological data in 1999).

Weaver and Lobkis (2001) demonstrated this conjecture for ultrasound waves by calculating that the long-term average of random noise in an aluminum block yields the time-domain impulse response between the two points. In 2002, they also provided one of the first proofs of Claerbout's conjecture. However, in order to prove it, they assumed that the noise wavefield was diffuse (i.e., waves arrive from all angles with equal strength). Diffusivity might be created approximately in nature by multiple scattering in a finite body with an irregular bounding surface, multiple scattering between randomly distributed scatterers within the body, or due to a random distribution of uncorrelated sources distributed throughout the medium. Nevertheless, the assumption of a diffuse wavefield imposes significant restriction on the domain of application of seismic interferometry.

In 2004, one of us (KW) proved the generalization of Claerbout's conjecture for 3D (acoustic and elastodymanic) media without assumptions about randomness of the medium, noise sources, or diffusivity of the wavefield. The derivation is based on reciprocity theory, and applies to any inhomogeneous, lossless, anisotropic medium. It uses independent responses of many sources (transient or noise) recorded at each pair of receivers to construct the inter-receiver impulse response, and for uncorrelated noise sources the expressions reduce to a single crosscorrelation of observations at the two receivers. This validated the interferometric conjecture of Claerbout.

Time reversal. In a pair of 2003 articles, Derode et al. showed how the principle of interferometry is related to time-reversed wavefields; in so doing they provided an intuitive and elegant derivation of impulse response reconstruction based entirely on physical, and not mathematical, arguments. They showed how a time-reversed mirror (a mirror that reflects any signal but with the time axis flipped) can be used to time-reverse a wavefield emitted from a single source, such that it converges on the original source location (imagine playing a movie backward such that ripples in a pond contract back to the point where a stone had been dropped into the water). If that wavefield is recorded at a second receiver location, the time-reversed impulse response between the source and receiver is recorded. The wavefield response to the original source of energy (the stone) is then reconstructed so the waves (ripples) begin to expand again; during this phase of the experiment the time-forward impulse response is recorded. It turns out that the operation of time reversal at the mirror is precisely the crosscorrelation operation that is used in seismic interferometry if instead sources were placed on the boundary rather than inside of the medium. Note that in Figure 1 (right), both time-forward and time-reversed impulse responses were constructed.

For direct source-receiver arrivals and for singly reflected waves, Snieder (2004, 2006) provided an explanation of the mechanism of impulse response reconstruction by crosscorrelation. Snieder argued that observable arrivals usually occur when the signal phase is stationary (approximately, does not change) with respect to perturbations of raypaths. Making this approximation allowed him to analyze the location of actual sources that contribute to the interferometric signal. He demonstrated that the dominant contribution to an interferometrically constructed, inter-receiver impulse response comes from scatterers (or noise sources) in two cones around extensions of the line that connects the two receivers. This implies that sources in other locations may be (approximately) redundant in the reconstruction.

Schuster (2001) and Schuster et al. (2004) showed how crosscorrelations of seismic responses from man-made or natural sources at the surface or in the subsurface can be used to form an image of the subsurface. The crosscorrelated data (interferograms) are downward extrapolated and imaged in much the same way as in standard prestack migration. The method is more robust than methods that first reconstruct the reflection response, and they make no assumptions with respect to wavefield diffusivity or sufficient source coverage. On the downside, most multiple reflections are incorrectly handled, and unwanted virtual multiples are generated—the latter appear as ghosts in the images.

Campillo and Paul (2003) produced the first account of geophysical, interferometric impulse response reconstruction using noise. They correlated seismic coda waves (which were assumed to be approximately diffuse due to multiple scattering) to estimate inter-receiver impulse responses. The reconstruction was only effective for the surface wave and direct arrival part of the impulse response (probably due to the near-surface distribution of common noise sources). Nevertheless, this was the main, practical breakthrough paper that encouraged geophysicists to consider using interferometric techniques in their fields.

Bakulin and Calvert (2004) produced the first practical application of seismic interferometry in an exploration setting. They showed for the first time that it is possible to create a virtual source at a subsurface receiver location (in a well) in practice. They measure the response of surface sources at downhole receivers. Using the virtual source methodology (crosscorrelating traces), they moved the sources (artificially) to downhole locations. This method has the potential to eliminate the imprint of the complex

overburden on the reflection response. The main restriction of the method is that it relies on the assumption that the downgoing primary wave at the buried receiver can be isolated from the total response which includes multiples.

The application of interferometrically constructed impulse responses for tomographic velocity inversion was shown by Shapiro et al. (2005) and by Sabra et al. (2005b). In applying the virtual source method, they crosscorrelated noise observations between many pairs of stations, thereby reconstructing the surface-wave components of impulse responses between these stations. Through tomographic velocity inversion, these surface waves were subsequently used to produce phase velocity maps indicating properties of the subsurface of southern California.

Computational wavefield modeling. Van Manen et al. (2005, 2006) showed how constructing impulse responses interferometrically on a computer provides an efficient and flexible, numerical waveform modeling scheme for heterogeneous, lossless media. By modeling the response of sources on a contour (or surface) around an arbitrary 2D (or 3D) medium, the response of any source recorded at any receiver entirely within this contour (or surface) can be obtained by crosscorrelation. This is particularly useful for nonlinear inversion or for modeling multiples, which require impulse responses between many combinations of source and receiver points within the medium. The authors also demonstrated that in a medium of any dimensionality it was necessary to store only waveforms generated by boundary sources in order to infer signals from wave propagation from any other source within the medium, and that to do otherwise was to store redundant data.

This resume of the history of interferometry shows that in a relatively small number of papers and mainly within the past six years, seismic interferometry has moved from being a field that was not popular and was based only on conjecture, to an active and extremely dynamic field in which huge theoretical and practical advances are being made almost monthly. Although we reported the advances as though they occurred in series, in fact the ideas developed more or less independently in different fields of science (ultrasonics, seismology, exploration geophysics, and oceanography). It was only in around 2003 that researchers in the different disciplines became aware of each other's work and began to see the links between them. The special supplement of GEOPHYSICS with its many additional advances is therefore timely, and below we present still further exciting examples that are published elsewhere.

Recent examples. We begin this section with two studies that focus on estimating aspects of Earth structure and properties, followed by three that focus on extracting and using novel types of waveforms using interferometry.

Example 1: Temporal change in velocity revealed from man-made explosions. In some applications, the goal of seismic interferometry is not to extract the impulse response of the medium from incoherent waves, but to determine the temporal change in the medium from these waves. Snieder et al. (2002) used the phrase *coda wave interferometry* for the interferometric measurement of temporal changes in the medium from strongly scattered waves. In order to do this one must have a repeatable source, but the source location and its signature need not be known.

Earthquake doublets are pairs of earthquakes with almost identical source mechanisms. The crosscorrelation of earthquake doublet records is a particular type of coda interferometry that is sensitive to differences in the medium that took place in between the occurrence of the pair of earthquakes.

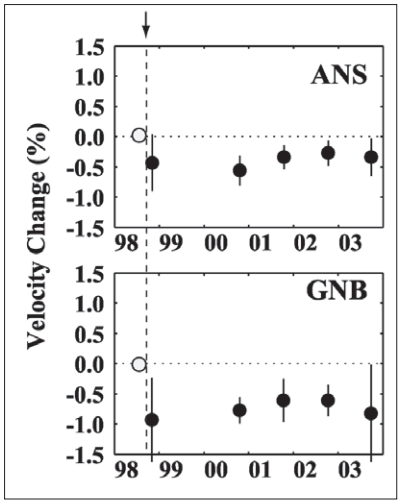

Figure 3. *Temporal change in velocity for 3–6 Hz at two sites near the M6.1 earthquake focal area of Iwate volcano, northeastern Japan, revealed from the repeated artificial explosion experiments. Solid circles represent the velocity change in % relative to a shot on 10 August 1998 (open circle), where vertical lines indicate one standard deviation. (Modified from Figure 8 of Nishimura, 2005.)*

Applying such an analysis to coda wave records of earthquake doublets before and after the occurrence of the 1979 Coyote earthquake in California, Poupinet et al. (1984) first revealed a velocity drop from the phase difference plot against lapse time. Taking this a step further, here we introduce recent observation of velocity change associated with an earthquake, and a recovery process during an interval of five years after the earthquake, as revealed by interferometry of records of repeated artificial explosions.

At Iwate volcano in northeastern Honshu, Japan, in early 1998, geophysicists found an inflation of the mountain topography and an increase of seismicity associated with a dike intrusion. An earthquake took place on the southwestern flank of the volcano on 3 September 1998.

Six similar, artificial explosions were detonated at the south end of the area beneath which the earthquake ruptured from August 1998 until 2003. Applying interferometry to seismic records from the artificial explosions recorded at eight seismograph stations around the focal area, Nishimura et al. (2000, 2005) found that the average seismic velocity of the crust in the frequency range of 3–6 Hz decreased by about 1% around the earthquake focal region. This velocity drop can be explained by the dilatation caused by the earthquake, if stress sensitivity of the percentage velocity change is of the order of 0.1/MPa. From the set of successive artificial explosion experiments, a gradual recovery of the seismic velocity toward its original value was observed over the next four years. Figure 3 shows temporal change in velocity at two sites near the focal area.

It is interesting this experimental study demonstrates the extreme sensitivity of interferometry to changes in the medium. While interferometry detected this 1% change in velocity, it was unidentifiable from traveltime analysis of first arrivals.

Example 2: Teleseismic surface-wave tomography across California. In crustal seismology, most seismic noise propagates as surface waves. By crosscorrelating long noise records from pairs of seismic stations it is possible to obtain the impulse response for surface waves traveling between the two stations. Seismic noise data from 148 broadband seismic stations in Southern California (Figure 4a) were used to extract the surface-wave arrival times between all station pairs in the network in the frequency band 0.05–0.2 Hz

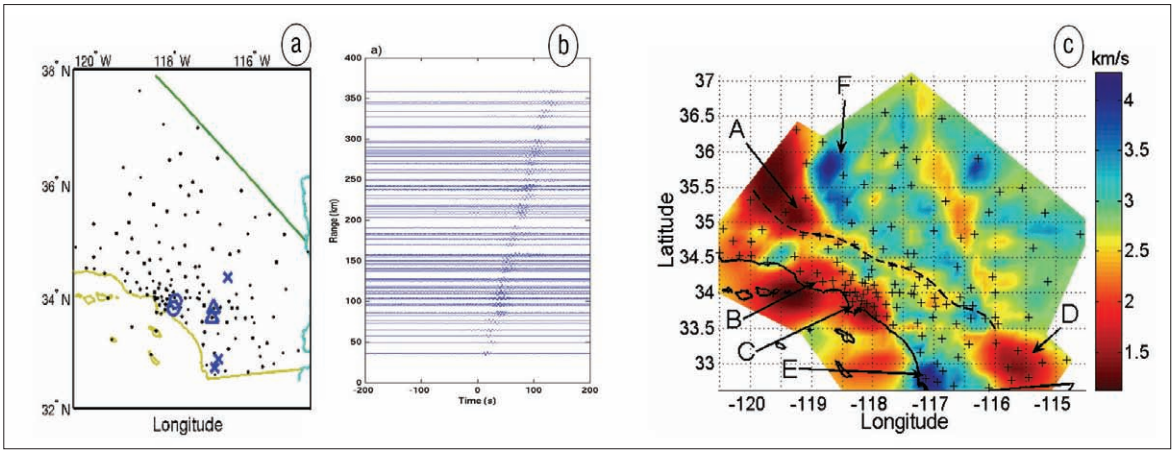

Figure 4. (a) Map of the 150 online stations in the Southern California Seismic Network. (b) Shot record generated from crosscorrelation of one month of the noise. (c) Surface-wave group velocity map for Southern California. (A = San Joaquin valley; B = Ventura; C = Los Angeles; D = Salton Sea Trough).

(Shapiro et al., 2005; Sabra et al., 2005a,b; Gerstoft et al., 2006). The station-pairs can be ordered into a so-called "passive shot" record indicating an outward-traveling wave (Figure 4b). In this area the seismic noise is strongly directionally biased, originating from the Pacific Ocean as ocean microseisms. For this reason a one-sided impulse response is obtained from interferometry of the noise (rather than an impulse response plus its time reverse as in Figure 1).

The seismic data were then used in a simple, but densely sampled tomographic procedure to estimate the surface-wave velocity structure for a region in Southern California (Figure 4c). The result compares favorably with previous estimates obtained using more conventional and elaborate inversion procedures. This study demonstrates that coherent ambient noise without an identifiable source can be used to create virtual sources at each of pairs of stations, and thereafter for seismic imaging purposes.

Example 3: Estimating building responses. Seismic interferometry is useful for extracting the response of structures, such as buildings, from the motion generated by an incoherent excitation. The left panel of Figure 5 shows the Robert A. Millikan Library in Pasadena, California. The right panel shows the horizontal component of the acceleration measured in the basement and the 10 floors after the Yorba Linda earthquake of 3 September 2002. At around t = 10 s, an impulsive S-wave strikes the building (blue box); at later times the building is excited by an extended surface-wave train (red box).

The waveforms in Figure 5 depend on (1) the mechanical properties of the building, (2) the excitation by the earthquake, and (3) the coupling of the building to the subsurface. Snieder and Safak (2006) separate the mechanical properties of the building from the excitation and the ground coupling by deconvolving the motion at all levels with respect to the motion at a given target level. (Here deconvolution is used rather than correlation because this operation eliminates the characteristics of the incoherent excitation more effectively than does correlation.) The result of deconvolving the waveforms of Figure 5 with respect to the waves recorded at the top floor is shown in Figure 6. In contrast to the original incoherent waves in Figure 5, the deconvolved waves in Figure 6 are coherent; they consist of the superposition of one upgoing wave and one downgoing wave. These waves can be used to measure the shear velocity and attenuation in the building.

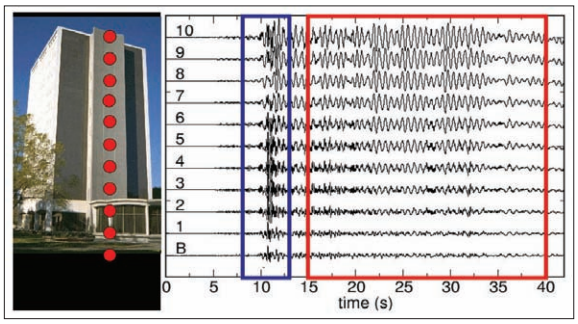

Figure 5. (left) The Robert A. Millikan Library in Pasadena, California, and the location of the accelerometers (red dots). The horizontal component of the acceleration after an earthquake is shown on the right. The red and blue boxes indicate the time intervals used for deconvolution.

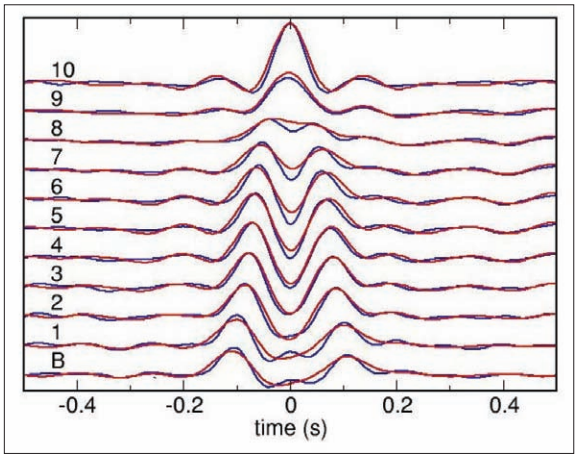

Figure 6. The waveforms obtained by deconvolving the waves at every level with the waves recorded at the top floor. Blue (red) lines indicate the waveforms obtained from the waves shown in the blue (red) boxes of Figure 5.

In fact, Snieder and Safak (2006) carried out the deconvolution process for the waves in the red box and the blue box in Figure 5 separately, and the corresponding deconvolved waves are shown in Figure 6 by red and blue lines,

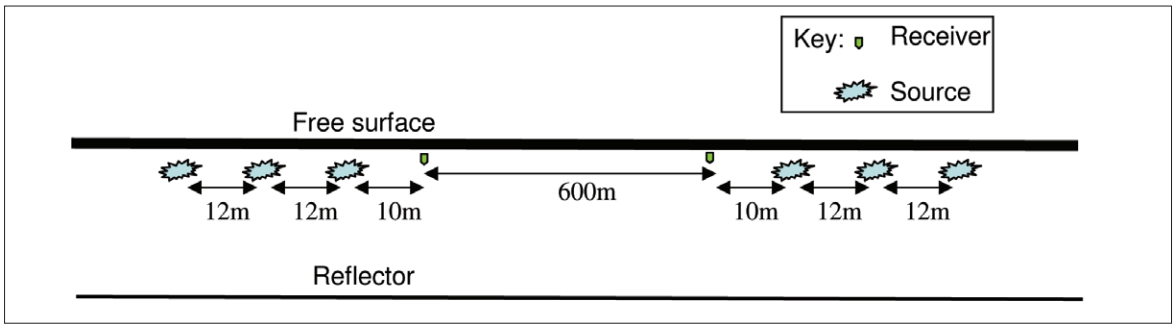

Figure 7. *Source and receiver pattern for the ground-roll experiments. The earth model consisted of a strongly attenuating medium including a single horizontal layer at depth of 20 m.*

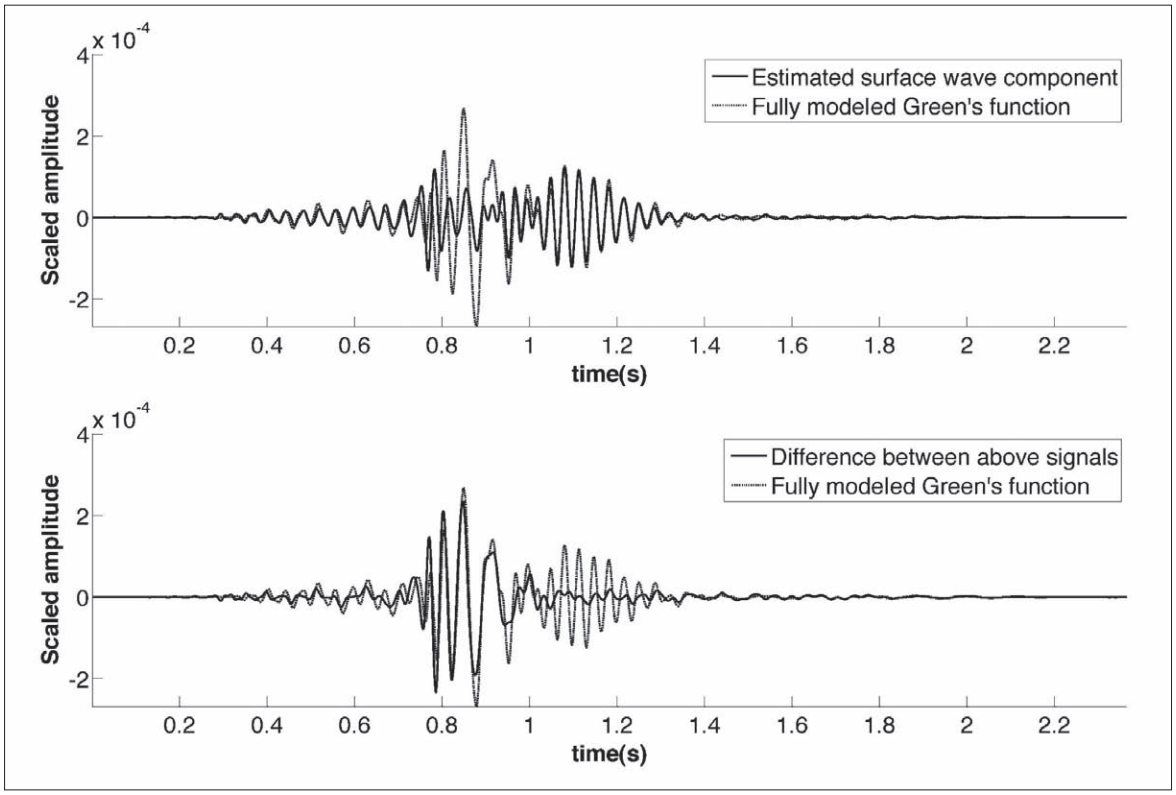

Figure 8. *Traces from experiment in Figure 7. (top) Dotted line is the true inter-receiver impulse response (Green's function), the solid line is the interferometrically constructed trace using only the sources in Figure 7. (bottom) Dotted line is same as top plot, the solid line is the difference between the curves in the top plot, i.e., the full impulse response with the interferometric trace subtracted.*

respectively. The original waveforms in the red and blue boxes of Figure 5 are quite different, yet the deconvolved waves are highly similar. These results show that this type of seismic interferometry does not depend strongly on the nature of the employed input signals.

Example 4: Ground-roll estimation and removal. We noted earlier that most practical studies using interferometry of background noise in the Earth successfully construct mainly surface and direct waves only, rather than reflected waves. This fact can be turned to our advantage.

Halliday et al. (2006) show that if the reason why this occurs is that typical noise sources in the Earth occur in the crust (i.e., near the surface), then it might be possible to reproduce this effect using artificial surface seismic sources. This would be achieved by crosscorrelating and integrating traces recorded at any pair of receivers from a set of surface seismic sources that completely surround the receivers on the surface only. The result would be seismic traces between a virtual source and receiver pair at the surface that contain dominantly the surface wave train, or ground roll.

This might seem like an odd thing to do—surface waves tell us nothing about the deep subsurface where reservoirs are situated. However, for exactly this reason ground-roll removal is a common and critical processing step for seismic data. After applying the method above, the interferometrically constructed ground-roll traces can be subtracted from real traces recorded when actual sources are placed at each of the virtual source locations. Thus, we should obtain

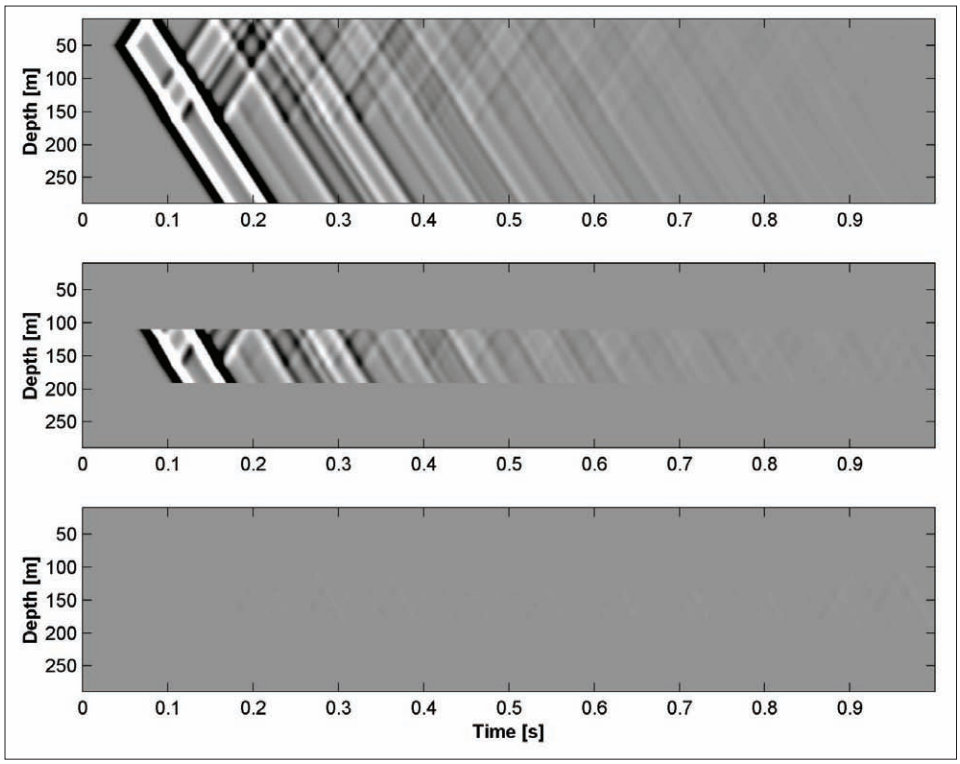

Figure 9. *Shot records for a vertical array in a 1D medium. (top) Full simulation over entire model. (middle) Local simulation around strong perturbation. (bottom) Difference between the two within the local region.*

seismic traces with ground roll removed.

Halliday et al. tested this on 2D synthetic acoustic and elastic examples of ground roll constructed in horizontally layered media, and media with complex near-surface topography, with and without realistic attenuation. Figures 7 and 8 show an acoustic example with a realistically attenuative medium that has only a single subsurface interface. Note that an equivalent theorem for interferometry in attenuative media has not been published to date; hence the interest in this example. Three surface sources were used to "surround" the receiver pair. The records from each source at the two receivers were crosscorrelated, and the results for the three sources were summed. The resulting interferogram, scaled by a positive constant factor, is shown at the top of Figure 8.

The arrivals in Figure 8 consist of a large body wave arrival that is the primary reflection (just before 1 s) and ground roll (after 1 s). The interferogram constructs the ground-roll component almost exactly, but not the body waves. Hence, the subtraction of the two top traces, shown in the lower plot, leaves the body waves intact but removes the ground roll.

There are several points to note about this example. First, although the structure is simple, it was not at all clear a priori that this method would work in an attenuative medium. Nevertheless, the results are impressive, as are those when using a more complex subsurface. The equivalent results for a nonattenuative medium are almost perfect.

Usually, so-called *f-k* filters are used to remove surface waves. However, these become increasingly ineffective as the recorded ground roll becomes more scattered from lateral reflectors or diffractors, because such scattering has the effect of spreading the ground roll over all wavevectors. On the other hand, given an appropriate source distribution, interferometry is equally effective for direct and scattered waves. This suggests that the new method of ground-roll removal could be equally effective in areas with complex near surface structures creating strong horizontal scattering—those in which *f-k* filtering fails.

Example 5: Exact waveform modeling after arbitrary changes in earth models. The example in Figure 1 shows that waveforms from sources distributed around the boundary of a medium contain sufficient information to obtain impulse responses from any source point in the interior of the medium. Van Manen et al. (2005, 2006a) show how this method can be generalized to both 2D and 3D, acoustic and elastic media, producing a flexible and efficient technique for waveform simulation.

Geophysical objectives often involve generating earth models for which signals from computer-simulated seismic wave propagation fit measured seismic waveform data. We simulate waveforms for a variety of earth models and check the data fit for each. Because each simulation typically requires powerful computing resources, the computational task of performing all of the simulations quickly becomes intractable unless intelligent tricks are employed and unrealistic limitations imposed on the modeling.

However, often we are interested to test data-fit for many models that differ only within some localized region, within a modeled reservoir for example. A class of sophisticated modeling techniques exists that allows approximate waveforms for the whole model to be calculated by simulating wave propagation only in a small subvolume, just large enough to contain the region that changed (these are called *wavefield injection methods*). While this reduces the computational task dramatically, the problem with such methods is that they employ something similar to what is commonly known as the Born approximation: they assume that if the model changes within the localized region, there will be no waves that interact with (reflect off or pass through) this altered part of the model more than once. Such multiple interactions always exist in the Earth and can significantly alter wave propaga-

tion, so estimated waveforms are always incorrect.

In a new development, van Manen et al. (2006b) have shown how to model exact waveforms after any local area of a model has been perturbed arbitrarily. This is significant because it means that the only times when it is necessary to simulate waveforms through a complete model are (a) once at the beginning through any reference model, and (b) for any model that differs from the reference model over the majority of its volume. If any model differs from the reference model only in a local area, then a local simulation around only that area is sufficient to obtain *exact* waveforms for the entire model.

Importantly, it turns out that the impulse responses between internal sources and receivers illustrated in Figure 1 are exactly those required to use this new method; constructing these impulse responses using the interferometric modeling methods of van Manen et al. makes this new method efficient and flexible.

Figure 9 shows an example in which waves in a 1D medium, similar to that in Figure 2b, were simulated after a large model perturbation within a region in the middle of the model's depth range. In the top panel the complete wavefield across the whole, perturbed model was simulated to obtain the true solution. In the middle panel, only a local simulation was performed around the perturbed area using the new method.

Provided the simulation in this local area matches that in the full simulation, the new method allows us to obtain the wavefield at any other point in the medium. All previous injection techniques would produce errors in the local simulation due to multiple interactions (e.g., between the perturbed area and the Earth's surface). However, the lower panel shows the difference between the top two panels within the local region, showing that the simulation using the new method is perfect.

The future. While the examples above and in the GEOPHYSICS supplement illustrate many theoretical developments and several applications that have already been found, some significant questions and challenges remain, and several currently uninvestigated areas of application show great promise for exploration and monitoring.

The challenges mainly concern extending the theory to account for real-world media and noise. First, we obtain only correct amplitudes in the traces derived from interferometry if the distribution of impulsive or noise sources is ideal in the sense that they illuminate the region of interest from all sides equally, and if the sources are uncorrelated. Natural sources do not satisfy these geometrical requirements and are often correlated, while active sources can never surround any portion of the Earth entirely (although this may not be necessary, see the discussion around Figure 2). Consequently a major challenge is to devise methods to obtain (approximately) dynamically correct waveforms from imperfect noise sources.

Second, all the theory described and used above assumes that the medium of propagation is lossless. No such medium exists in the natural Earth, so there is a need to generalize the theory to account for attenuative media.

A third theoretical question is the following: most of the theory above was derived using crosscorrelations. However, there are situations in which deconvolution seems a more natural operation to apply—indeed it was applied in the Millikan Library example. Given that the only general proof of Claerbout's conjecture that exists was based around correlational representation theorems, is there a version of the theory based around deconvolution instead? If so, under what conditions should it be applied?

There are three main areas of application that would seem to be promising for the exploration industry. First, in principle the theory above can be applied directly to obtain impulse responses for multicomponent (MC) source and receiver surveys across a region using only MC receivers. The MC sources are created virtually by interferometry. Campillo and Paul (2003) showed that for crustal surface waves the 3×3 impulse response tensor can be determined from interferometry. Since one of the main barriers to nine-component surveys is the cost of MC sources, this would seem to be a way forward to reduce this cost. Clearly experiments are needed to test this hypothesis.

Second, the examples above show that interferograms constructed by crosscorrelating coda waves recorded at different times are extremely sensitive to small changes in the medium that occurred between recordings. This would seem to have obvious application to time-lapse seismic monitoring where changes in reservoir fluids may have very small impact on the acoustic impedance.

Third, we have mainly presented seismic applications, but presently the theory applies equally to (lossless) electromagnetic wave propagation. This possibility has barely been developed within the exploration industry but would seem promising given the recent upsurge in interest of time-domain EM methods for fluid discrimination, and its use for near-surface geophysics.

Principal message. The principal message in this article is that seismic interferometry is worth watching closely. This field shows great promise, is developing rapidly compared to other areas of seismology, and is still in its infancy. Given this context and the current level of interest, it is a safe bet that further theoretical breakthroughs and the first commercially attractive applications are around the corner. TLE

Acknowledgments: We thank the office of Basic Energy Sciences of the Department of Energy for sponsoring a workshop on "Advanced Noninvasive Monitoring Techniques" in Houston in November 2005, at which this publication was proposed.

Corresponding author: Andrew.Curtis@ed.ac.uk

Appendix. Because this is a review article which cites several papers originally published in journals not specifically dedicated to geophysics, the list of references is more extensive than for the typical *TLE* article and are in the form typically used by an archival journal rather than *TLE*'s standard "Suggested reading" style.

Bakulin, A., and R. Calvert, 2004, Virtual source: new method for imaging and 4D below complex overburden: 74th Annual International Meeting, Society of Exploration Geophysicists, *Expanded Abstracts*, 2477–2480.

Callen, H. B. and T. A. Welton, 1951, Irreversibility and generalized noise, *Physical Review*, 83, 1231–1235.

Campillo, M., and A. Paul, 2003, Long-range correlations in the diffuse seismic coda: *Science*, 299, 547–549.

Claerbout, J. F., 1968, Synthesis of a layered medium from its acoustic transmission response: GEOPHYSICS, 33, 264–269.

Derode, A., E. Larose, M. Campillo, and M. Fink, 2003a, How to estimate the Green's function of a heterogeneous medium between two passive sensors? Application to acoustic waves: *Applied Physics Letters*, 83, no. 15, 3054–3056.

Derode, A., E. Larose, M. Tanter, J. de Rosny, A. Tourin, M. Campillo, and M. Fink, 2003b, Recovering the Green's function from field-field correlations in an open scattering medium (L): *Journal of the Acoustical Society of America*, 113, no. 6, 2973–2976.

Gerstoft, P., K. G. Sabra, P. Roux, W. A. Kuperman, and M. C. Fehler, 2006, Green's functions and surface wave tomography from microseisms in Southern California, in press GEOPHYSICS.

Halliday, D., A. Curtis, D.-J. van Manen, J. O. A. Robertsson, 2006, On Interferometric surface wave isolation, *Geophysical Research Letters*, Submitted.

Nishimura, T., N. Uchida, H. Sato, M. Ohtake, S. Tanaka, and H. Hamaguchi, 2000, Temporal changes of the crustal structure associated with the M6.1 earthquake on September 3, 1998, and the volcanic activity of Mount Iwate, Japan, *Geophysical Research Letters*, 27, 269–272.

Nishimura, T., S. Tanaka, T. Yamawaki, H. Yamamoto, T. Sano, M. Sato, H. Nakahara, N. Uchida, S. Hori, and H. Sato, 2005, Temporal changes in seismic velocity of the crust around Iwate volcano, Japan, as inferred from analyses of repeated active seismic experiment data from 1998 to 2003, *Earth Planets Space*, 57, 491–505.

Poupinet, G., W. L. Ellsworth, and J. Frechet, 1984, Monitoring velocity variations in the crust using earthquake doublets: An application to the Calaveras fault, California, *Journal of Geophysical Research*, 89, 5719–5731.

Rickett, J., and J. Claerbout, 1999, Acoustic daylight imaging via spectral factorization: Helioseismology and reservoir monitoring: THE LEADING EDGE, 18, 957–960.

Sabra, K. G., P. Gerstoft, P. Roux, W. A. Kuperman, and M. C. Fehler, 2005b, Surface wave tomography from microseisms in Southern California: *Geophysical Research Letters*, 32, L14311-1–L14311-4.

Sabra, K. G., P. Gerstoft, P. Roux, W. A. Kuperman and M. C. Fehler, 2005a, Extracting time-domain Green's function estimates from ambient seismic noise, *Geophysical Research Letters*, 32, doi:10.1029/2004GL021862.

Schuster, G. T., 2001, Theory of daylight/interferometric imaging: tutorial: 63rd Meeting, European Association of Geoscientists and Engineers, *Extended Abstracts*, Session: A32.

Schuster, G. T., J. Yu, J. Sheng, and J. Rickett, 2004, Interferometric/daylight seismic imaging: *Geophysical Journal International*, 157, 838–852.

Shapiro, N. M., M. Campillo, L. Stehly and M. H. Ritzwoller, 2005, High-resolution surface wave tomography from ambient seismic noise, *Science*, 307, 1615–1617.

Snieder, R., 2004, Extracting the Green's function from the correlation of coda waves: A derivation based on stationary phase: *Physical Review E*, 69, 046610-1–046610-8.

Snieder, R., A. Gret, H. Douma, and J. Scales, 2002, Coda wave interferometry for estimating nonlinear behavior in seismic velocity, *Science*, 295, 2253–2255.

Snieder R. and E. Safak, Extracting the building response using seismic interferometry; theory and application to the Millikan Library in Pasadena, California, *Bulletin of the Seismological Society of America*, 96, 586–598, 2006.

Snieder, R., K. Wapenaar, and K. Larner, Spurious multiples in seismic interferometric imaging of primaries, GEOPHYSICS, in press, 2006 (Special issue).

van Manen, D.-J., J. O. A. Robertsson, and A. Curtis, 2005, Modeling of wave propagation in inhomogeneous media: *Physical Review Letters*, 94, 164301-1–164301-4.

van Manen, D.-J., A. Curtis, and J. O. A. Robertsson, 2006a, SI183–SI196.

van Manen, D.-J., J. O. A. Robertsson, and A. Curtis, 2006b, On long range interactions of waves in heterogeneous media: *Science*, Submitted.

Wapenaar, K., 2004, Retrieving the elastodynamic Green's function of an arbitrary inhomogeneous medium by crosscorrelation: *Physical Review Letters*, 93, 254301-1– 254301-4.

Weaver, R. L., and O. I. Lobkis, 2001, Ultrasonics without a source: Thermal fluctuation correlations at MHz frequencies: *Physical Review Letters*, 87, 134301-1–134301-4.

DOI:10.1190/1.9781560801924.ch2

Virtual Surface Seismic Data from Downhole Passive Arrays

Gerard Schuster (University of Utah)

ABSTRACT

Monitoring oilfield reservoirs by downhole seismic arrays typically consists of picking traveltimes of direct arrivals and locating the hypocenter of the fracturing rock. The 3-component array typically has no more than a handful of geophones located in one or more wells. To broaden the use of this downhole recording array I propose that it can, in principle, also be used to record 3D VSP data from controlled surface sources. These VSP data with free surface multiples can then be interferometrically transformed into virtual surface seismic reflection data, so that the subsurface reflection coverage is almost the same as a surface seismic experiment. To support this proposal, I present interferometric imaging results from 2D and 3D VSP data. Images from free surface related multiples show that the subsurface reflection illumination is almost as wide as that of a surface seismic experiment and is much larger than that from a conventional VSP image.

INTERFEROMETRIC IMAGING OF VSP MULTIPLES

Multiples have traditionally been considered as coherent noise, and so much effort has been put into developing dereverberation algorithms. However, our point of view is that multiple reflection energy can often be used to better illuminate the subsurface compared to primary reflection imaging. As an example, Figure 1 depicts the subsurface illumination provided by primary reflections recorded with VSP receivers in a well (also see related ray diagrams in Figure 2). Even though the frequency content in VSP data is more than twice that of surface seismic profile (SSP) data, a narrow cone of coverage does not always justify the expense of a VSP survey. But if the reflections from free-surface multiples are migrated then the coverage is almost as wide as a 3D SSP survey (see Figure 1).

A problem with free-surface multiple migration is that the path lengths are often more than twice that of the primary reflection ray. This means that the multiple reflection will have lower signal-to-noise, be distorted more by static errors (multiples making more than one round trip to the free surface) and suffer more than twice the migration velocity error of a primary reflection.

To mitigate some of the above problems, we have developed interferometric imaging (II) to migrate multiple reflection and scattering energy (Schuster et al., 2004). We demonstrate the effectiveness of II with both synthetic and field data, and show that II of VSP data provides significantly more coverage than traditional VSP imaging of primary reflections. Moreover, the timing distortions due to migration velocity errors and static distortions at

Reprinted with permission from EAGE Workshop, Passive Seismic: Exploration and Monitoring Applications, A24.

the well are significantly reduced. The main idea for interferometric imaging of free-surface

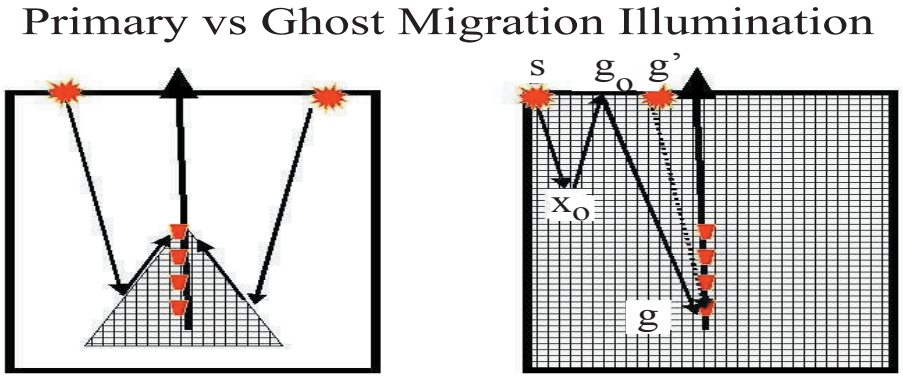

Figure 1: VSP primary reflections provide a narrow hatched cone of coverage compared to the nearly full hatched illumination given by source-side ghosts (from Jiang et al., 2005).

multiples in passive seismic data was initiated by Rickett and Claerbout (1999) and later extended to VSP data by Schuster (2001) and Yu and Schuster (2006). A related concept is interferometric redatuming, as illustrated in Figure 2a. Here, the correlation of two direct waves, the $d(\mathbf{B}|\mathbf{A},t)$ trace recorded at $\mathbf{B}$ and the $d(\mathbf{C}|\mathbf{A},t)$ recorded at $\mathbf{C}$, results in the trace $d(\mathbf{C}|\mathbf{B},t)$ with a redatumed direct wave[1].

Mathematically, we are saying $d(\mathbf{B}|\mathbf{A},t) \otimes d(\mathbf{C}|\mathbf{A},t) \approx d(\mathbf{C}|\mathbf{B},t)$ is a trace that is kinematically identical to one obtained from a virtual source at $\mathbf{B}$ and a geophone at $\mathbf{C}$; here, $\otimes$ denotes temporal correlation. This makes sense because correlating $d(\mathbf{B}|\mathbf{A},t)$ with $d(\mathbf{C}|\mathbf{A},t)$ shifts the direct arrival in $d(\mathbf{C}|\mathbf{A},t)$ by the amount of time to go from $\mathbf{A}$ to $\mathbf{B}$. The main advantage in this approach is that the sources and receivers are closer to the target of interest, which typically means better spatial resolution of the target's properties. The source statics and the distorting effects of the medium between $\mathbf{A}$ and $\mathbf{B}$ are avoided by redatuming the sources to $\mathbf{B}$, and no velocity model is needed!

The extension of this concept to inverse VSP data is shown in Figure 2b, where the direct arrival $d(\mathbf{C}|\mathbf{A},t)$ recorded at $\mathbf{C}$ is correlated with the ghost arrival $d(\mathbf{C}|\mathbf{A},t)^{ghost}$ at $\mathbf{C}$ to give the redatumed trace $d(\mathbf{C}|\mathbf{C},t)^{primary} \approx d(\mathbf{C}|\mathbf{A},t) \otimes d(\mathbf{C}|\mathbf{A},t)^{ghost}$. In this case, we can say that the multiple reflections have been kinematically redatumed to be zero-offset primary reflections $d(\mathbf{C}|\mathbf{C},t)^{primary}$ associated with a surface seismic experiment. For non-zero offset data, this idea is still valid if the correlated data are summed over all buried

[1]The notation $d(\mathbf{B}|\mathbf{A},t)$ indicates that the source is at position $\mathbf{A}$ and the receiver is at $\mathbf{B}$, and t represents listening time for a source initiated at time $t=0$.

sources along the well i.e., $d(\mathbf{C}|\mathbf{C}',t)^{primary} \approx \sum_A d(\mathbf{C}|\mathbf{A},t) \otimes d(\mathbf{C}'|\mathbf{A},t)$ (Schuster et al., 2004). These equations are also true for VSP data because the source and receivers can be interchanged by reciprocity.

NUMERICAL EXAMPLES

Synthetic and field data examples are used to illustrate the possibility of using a downhole passive seismic array to interferometrically obtain virtual surface seismic data.

Dipping Layer Model. The first example is the dipping layer model, with interfaces indicated by the solid dipping lines in Figure 3a. Here, a finite-difference method was used to generate 92 VSP shot gathers, each with 50 traces. The well is along the leftmost vertical axis in the model, shot spacing on the surface was 10 m and there are 50 receivers evenly distributed between the depths of 550 m and 950 m in the vertical well. For the interferometric imaging, only traces from eight receivers (20 m spacing) are used with the top receiver at the depth of 550 m.

Figure 3b shows the migration section obtained from the primary reflections, and Figure 3c shows the section obtained by only using eight shot gathers to interferometrically migrate the downgoing first-order multiple. We can see that the multiples image provides both a taller and wider coverage of the subsurface reflectivity compared to the primary reflection image. The structures above the receivers are illuminated by the multiples, which are invisible to the primary reflections. For the interferometric image, only eight traces/shot gather were used compared to 50 traces/shot gather for the primary migration image. This suggests a handful of downhole geophones can be used for widespread reflection coverage of the subsurface.

2D VSP Multiple Migration vs SSP Migration of Marine Data. A 3D VSP marine data set was recorded using 12 receivers between the depths of 3.6 km and 3.72 km. Data associated with one radial line of shots were used to migrate the ghost reflections to give the image in Figure 4a. A section obtained by migrating primary reflections in SSP data collected over the same area is shown in Figure 4b. Both images show a similar reflectivity distribution, with the VSP data with about 1.5 times the temporal resolution of the SSP data. The ghost image used a mirror imaging condition rather than interferometric migration. Nevertheless, this image compared well with the SSP image and appeared to be of higher frequency than the SSP data. The receivers were mostly below the image area so the reflectivity shown in Figure 4a is normally unseen by traditional migration of VSP primary reflections.

3D Interferometric Migration of VSP Marine Data. For a VSP experiment, Figure 1

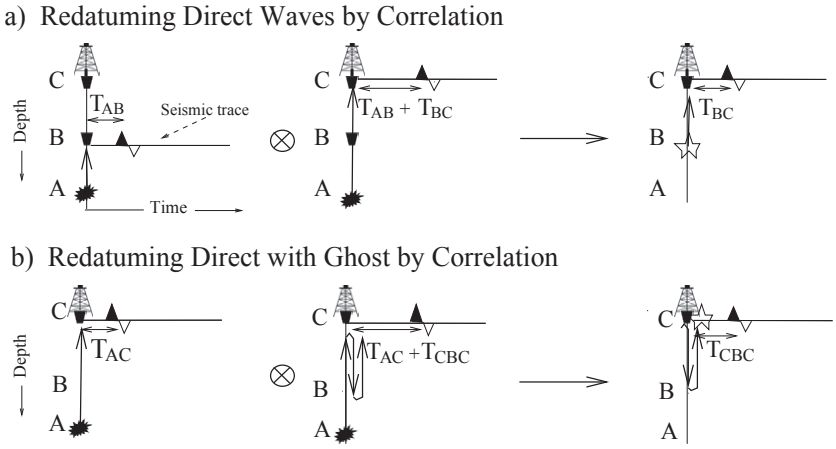

Figure 2: a) For a buried source at **A**, the direct wave recorded at **B** (left diagram) correlated with the direct wave (middle diagram) recorded at **C** yields a redatumed direct wave (right diagram) where the source is relocated to **B**. The $\otimes$ denotes the correlation of one trace with the other. b). Same as a), except direct wave recorded at **C** (left diagram) is correlated with a ghost reflection recorded at **C** (middle diagram) to yield a primary reflection (right diagram) for a source at **C** and receiver at **C**.

shows that the illumination area of VSP primaries is much less than that of VSP multiples (Jiang et al., 2005). This wider illumination is dramatically demonstrated in Figure 5, which is the interferometric image obtained from 3D marine VSP data (He, 2006) recorded by a few dozen receivers in the vicinity of the well symbol. After correlation and summation of the VSP traces, one VSP receiver gather has been transformed to be many surface CSGs, with nearly the same coverage as a surface SSP experiment. For comparison, the reflectivity distribution above the Figure 5 VSP geophone is invisible to standard imaging of VSP primaries.

SUMMARY and DISCUSSION

I proposed the possibility of using downhole passive seismic arrays as a means for obtaining virtual surface seismic data. The resulting redatuming and migration procedure is known as interferometric imaging of free surface multiples, and the implication is that existing downhole passive arrays can be used to monitor a much larger area of a reservoir by employing surface seismic surfaces. The feasibility of such an approach is suggested by the successful imaging of both synthetic data and field VSP data using a small number of geophones. I am grateful for support from the UTAM consortium (http://utam.gg.utah.edu).

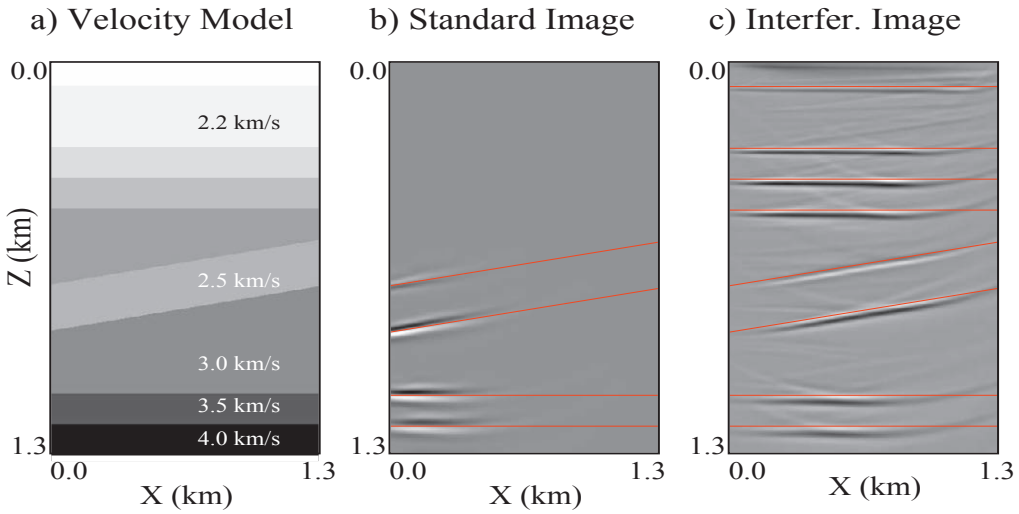

Figure 3: a) Dipping layer velocity model, b) VSP primary migration image, and c) interferometric VSP migration image; 92 sources are on the surface and receivers are evenly distributed along the leftmost vertical axis. Solid lines denote actual reflector positions (Jiang et al., 2005).

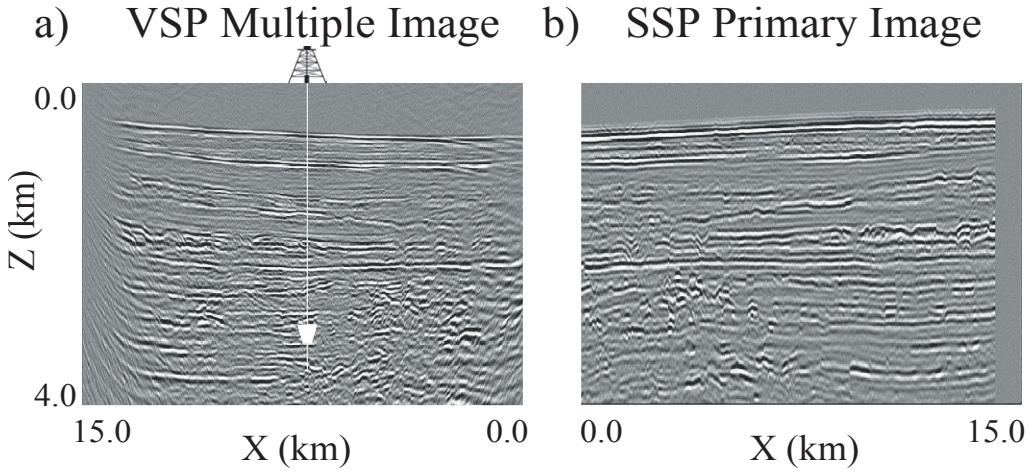

Figure 4: Migration images obtained by migration of a) ghosts in 3D VSP marine data and b) primary reflections in 3D SSP data over the same area (Jiang et al., 2005).

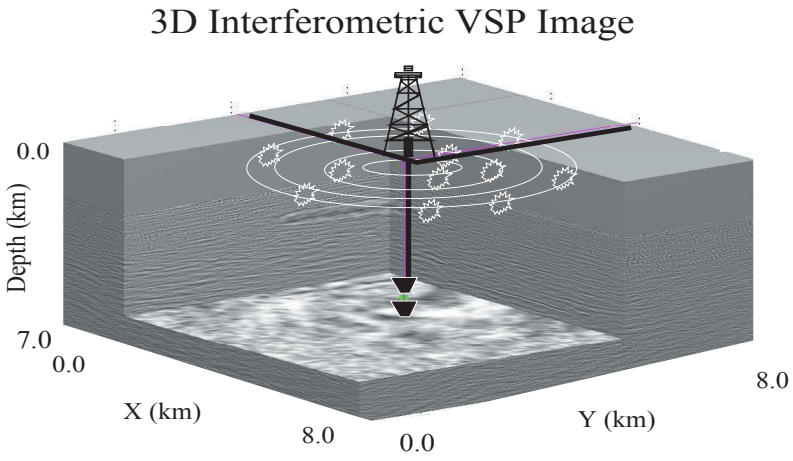

Figure 5: 3D VSP image of free-surface multiples after wave equation migration for one VSP receiver gather and thousands of shots on the sea surface (He, 2006).

REFERENCES

He, R., 2006, Wave equation interferometric migration of VSP data: PhD dissertation, U. of Utah.

Jiang, Z., Yu, J., Hornby, B., and Schuster, G.T., 2005, Migration of multiples: The Leading Edge, 315-318.

Rickett, J., and Claerbout, J., 1999, Acoustic daylight imaging via spectral factorization: Helioseismology and reservoir monitoring: The Leading Edge, 18, 957-960.

Schuster, 2001, Seismic interferometry: Tutorial: 63rd Annual EAGE meeting, Expanded Abstracts.

Schuster, G.T., Yu, J., Sheng, J., and Rickett, J., 2004a, Interferometric/daylight imaging: GJI, **157**, 838-852.

Yu, J. and Schuster, G.T., 2006, Crosscorrelogram migration of inverse vertical seismic profile data: Geophysics **71**, S1-S11.

Virtual source applications to imaging and reservoir monitoring

A. Bakulin, A. Mateeva, K. Mehta, P. Jorgensen, J. Ferrandis, I. Sinha Herhold, and J. Lopez, Shell International Exploration & Production, Houston, USA

The virtual source method is a breakthrough that allows us to image and monitor the subsurface in cases where surface seismic or VSP fail to deliver. In settings where the overburden is complex or changing, traditional time-lapse signals are weak or nonrepeatable, leading to ineffective seismic input to reservoir modeling and little of value generated by repeated seismic surveys. On the other hand, the virtual source method allows us to image under complex overburden, yields repeatable data for reservoir monitoring, enables shear seismic, and may help us "look ahead" as we drill.

Virtual source technology circumvents overburden-induced problems by synthesizing controllable sources at the locations of sensors placed underneath complicated or changing overburden. This results in a buried seismic survey with fixed source and receiver locations that illuminates the underlying reservoir section. These virtual sources can harness all kinds of scattered energy that reaches them (P or S) and as such are completely data-driven. We don't need to know any details of the overburden to create them.

Shell operating units have used virtual source technology in exploration wells in the deepwater Gulf of Mexico to look ahead and pinpoint drilling hazards and image reservoirs with high resolution. Cost benefits can be substantial, given that each drilling incident or geologic sidetrack can cost US$5–10 million. Repeatable virtual sources are critical to enhance the sensitivity of time-lapse seismic in areas of low signal, to increase hydrocarbon recovery, and to unlock the potential of unconventional resources. We illustrate these advances through a series of field examples and discuss opportunities for wider deployment and the practical issues that need to be overcome.

Basic concept. While many formal derivations of the technique have appeared in the literature, for the geophysical practitioner, the logic depicted in Figure 1 seems to best capture the essence of the virtual source method, as it is explained below through a reverse-time experiment.

Professor Fink and colleagues at the École Supérieure de Physique et de Chimie Industrielles de la Ville de Paris focus acoustic energy at a point (R_α) using a surface array of actuators (S_k) that send time-reversed signals of original recordings from a real source at the target location (R_α). They call the actuator array a time-reversal mirror, as the energy back-propagation requires no knowledge of the medium and, in fact, the more complex the medium the better the focusing. Such reverse-time focusing is routinely applied in the medical field for the treatment of kidney stones, brain tumors, and other abnormalities.

The virtual source method goes two steps beyond the reverse-time acoustic experiments. First, it recognizes that, after focusing at the target location, energy reradiates from this focal point (not an energy sink) that we call a virtual source. Second, it recognizes that propagation from the virtual source onward approximates that from a real source at this point (R_α). Therefore, we can use the wavefield radiated from the virtual source location to image the surrounding medium just as we would use the wavefield from a physical source at that point. To create a virtual source below the surface of the Earth using seismic data, we need

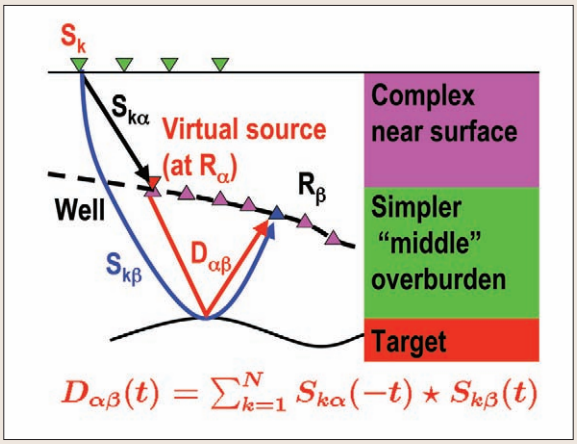

Figure 1. *Schematic of virtual source method.*

a VSP-type experiment. In a VSP survey, we have sources where Fink et al. had actuators (S_k) and a receiver where they had a physical source (R_α). Using reciprocity and linearity, we can turn the VSP data around and computationally create a virtual source at R_α.

From a processing standpoint it suffices to visualize the technique as a cross-correlation of direct-arrival energy at one buried geophone (the virtual source) with the trace recorded at a second geophone (the receiver). The result, once summed over a suitable set of illuminating physical sources, approximates the response of a buried source-receiver pair in the subsurface. This data-driven virtual source redatuming process does not require any velocity information.

A word on artifacts and unwanted arrivals. In theory, extracting the exact response between a virtual source and a receiver requires illumination by physical sources that completely surround the area of interest. In practice, we have a limited aperture from surface-source acquisition. In addition, we may want to limit the type and directionality of the arrivals that fuel the virtual source in order to make it emit a preferred mode (P or S) in a desired direction (e.g., downward). In either case, limiting the input to the virtual source computation creates some artifacts in the virtual source data—namely, spurious events that would have been canceled if we had sources all around. Given that we cannot cancel them, we may try to avoid exciting them by further limiting the input to the virtual source by wavefield separation combined with gating. This strategy can be also employed to suppress other unwanted events such as interbed multiples.

Here is an example with an ocean-bottom cable (OBC) survey from Mars Field in the Gulf of Mexico. Virtual source redatuming to the seabed at Mars is aimed at improving repeatability of time-lapse surveys by eliminating the effects of varying water depth and velocity, and imperfect acquisition. Figure 2 shows the result of turning the middle OBC receiver into a virtual source in three slightly different ways. Correlating the total wavefields at the virtual source and receiver locations, as is a common practice in seismic inter-

Reprinted from The Leading Edge, **26**, 732–740.

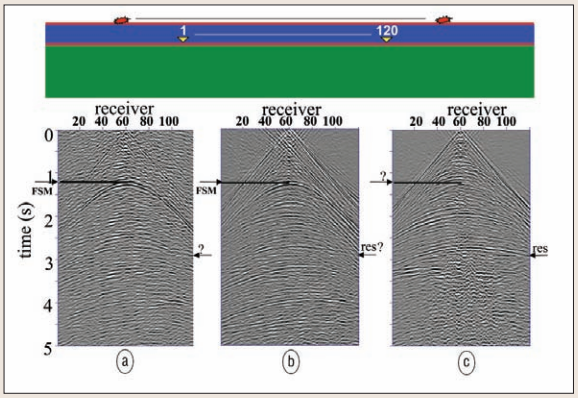

Figure 2. *Suppressing noise in the redatumed Mars OBC survey; common virtual shot gathers created by cross-correlating: (a) total wavefields at virtual source and receiver locations; (b) total wavefields but with the time-reversed wavefield gated on first arrivals; (c) downgoing waves at the virtual source location (gated on first arrivals) with the upgoing waves at the receiver.*

ferometry, we observe a strong free-surface multiple (FSM) and unwanted artificial events caused by incomplete aperture (Figure 2a). Doing the same but with a gate on the first arrival on the time-reversed wavefield cleans up the virtual source data and diminishes the amplitude of free-surface multiples (Figure 2b). This is our current most used practice. An even better practice is to correlate the downgoing waves at the virtual source (gated to first arrivals) with the upgoing waves at the receiver. One can see much better suppression of free-surface multiples, cleaner shallow reflections and enhanced reservoir response (Figure 2c).

Such adaptations of the virtual source construction make it very usable for seismic prospecting. They allow us great control on the radiation pattern and properties of the virtual source wavefield—an area that deserves additional study. Here we advocate an experimental approach and explore a number of applications based on physical intuition and business needs. Perhaps our results will inspire further efforts into understanding the theoretical underpinnings of these practical applications.

Virtual check shot. A simple application of virtual source technology involves propagation from one geophone to another (along the geophone string), a configuration that can be used to accurately estimate velocities along the borehole. Compared to conventional check shots with a single source at the surface, virtual check shots have virtual sources in the borehole and are immune to raypath distortions in the overburden. By appropriate gating on VSP traces, one can create virtual sources that emit predominantly compressional (P) or shear (S) waves that are detected on the vertical or horizontal components in the geophones below. A walkaway VSP in the deepwater Gulf of Mexico with geophones in and below salt was used to test this concept. The resulting velocity profiles for P- and S-waves were in very good agreement with sonic logs below salt at a depth of about 22 000 ft (Figure 3). Velocity estimates in salt were also in excellent agreement with well velocities.

Virtual check shots may be used where traditional check shots are expected to be inaccurate (e.g., because of complex overlying salt geometry) or unavailable (e.g., shear check shot), or where sonic logs are not feasible or desirable (e.g., in large boreholes or nonreservoir sections). These may be repeated over time to identify velocity variations

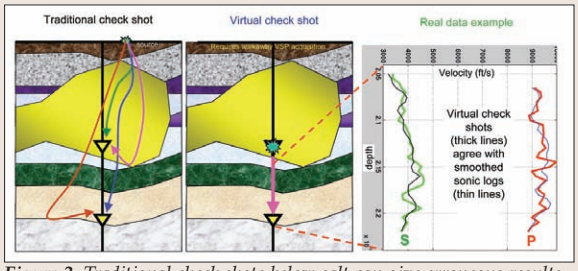

Figure 3. *Traditional check shots below salt can give erroneous results because of complex raypaths and distorted waveforms. A virtual check shot with a virtual source location in the borehole avoids these complications. It gives accurate results below massive salt, as seen in the example on the right.*

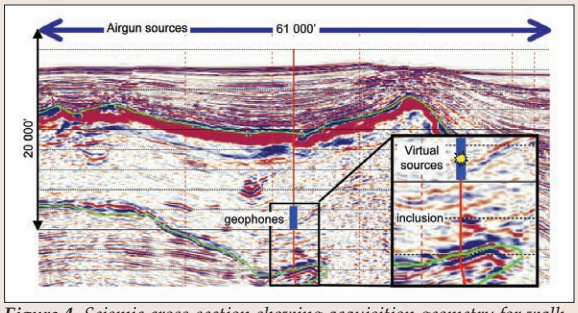

Figure 4. *Seismic cross-section showing acquisition geometry for walkaway VSP in deepwater Gulf of Mexico prospect. The VSP was acquired in 40 geophones spanning a 2000-ft interval in the borehole. The inset shows the main objective of the virtual source analysis: high-resolution characterization of the in-salt inclusion and the base of salt interface.*

due to geomechanical effects in producing fields, as measured at seismic frequencies. If downhole sensors are installed permanently, anomalies in virtual check shots may provide early warning of potential casing integrity problems.

Look-ahead VSP. Virtual sources can be synthesized underneath massively distorting features (such as salt, basalt, or ice) and processed to obtain high-resolution images of the reflectors below, regardless of the overlying complexities. For a single instrumented well bore drilled along geologic dip, the lateral extent of the resulting 2D image is ultimately limited by sensor coverage, and otherwise depends critically on the relative inclination of the well to reflectors. The image dimension is maximized for wells parallel to reflectors—e.g., horizontal wells over flat geology or vertical wells next to steeply dipping beds. This dimension is reduced proportionally as the angle between well and reflector increases, and shrinks to a single trace for wells perpendicular to reflectors, as in the case of a look-ahead VSP that we discuss next.

The look-ahead VSP with virtual sources was tested on a walkaway VSP data set acquired while a well was being drilled through thick salt in the Gulf of Mexico. The objective was to obtain a high-resolution image of the path ahead, which surface seismic suggested was plagued with intrasalt hazards, and of a complex base of salt interface with a potential for highly overpressured sands immediately below salt (Figure 4).

The VSP data set consisted of 40 geophones at 50-ft spacing, which were transformed into 40 virtual sources, giving a total of 1600 source-receiver pairs illuminating a narrow path ahead of the well. This high-fold data set confirmed

that a prominent seismic feature in the salt was indeed an intrasalt reflection and not a multiple from the surface seismic. Careful study of the virtual source gathers allowed one to estimate the dip, attitude, and time of the intrasalt reflector. A salt velocity estimate from the corresponding virtual check shot yielded a prediction to the depth of the reflector 2000 ft ahead of the well with 50-ft uncertainty; the prediction was communicated to the rig, which soon thereafter encountered the inclusion within 2 ft of prognosis (Figure 5).

A similar analysis yielded a prediction for the depth to base of salt 4000 ft ahead of the well with 70-ft uncertainty. This prediction was also validated by the well results. Further dissection of the base salt reflection on the virtual source data revealed a bright event just 350 ft below salt, suggestive of hydrocarbons, which the well also validated (Figure 5).

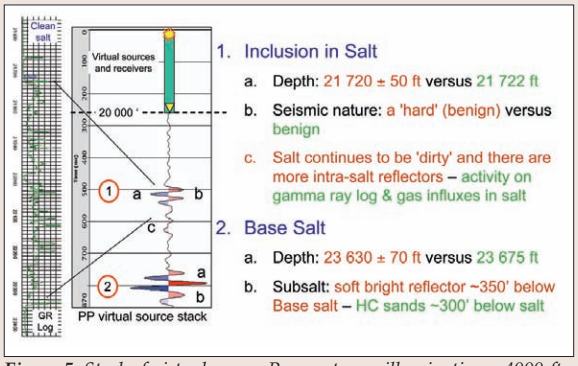

Figure 5. Stack of virtual source P-wave traces illuminating a 4000-ft interval ahead of the well. Comparison of high-resolution predrill predictions (red) with postdrill results (green) validates the remarkable accuracy of the virtual source data.

Imaging under complex overburden. Next, we illustrate the advantages of virtual source technology to generate useful images with some lateral extent, in a model inspired by the Peace River field in Canada (Figure 6a). A very heterogeneous near-surface layer creates large distortions of the seismic wavefield recorded on downhole receivers in a horizontal well above the reservoir (Figure 6b). These distortions cannot be handled by conventional imaging methods, as the requisite high-resolution near-surface velocity field cannot be recovered from the data itself. However, by applying the virtual source method, we immediately remove most of these distortions and obtain a virtual source gather (Figure 6c, in black) which is kinematically simple and closely resembles the ground truth response of an actual buried source (Figure 6c, in red) that we wanted to replicate. The virtual source data can then be easily migrated with a 1D velocity model beneath the horizontal well (Figure 6d). The virtual source image is of excellent quality and compares favorably to the idealized case of a conventional VSP image obtained with the exact velocity model (Figure 6e).

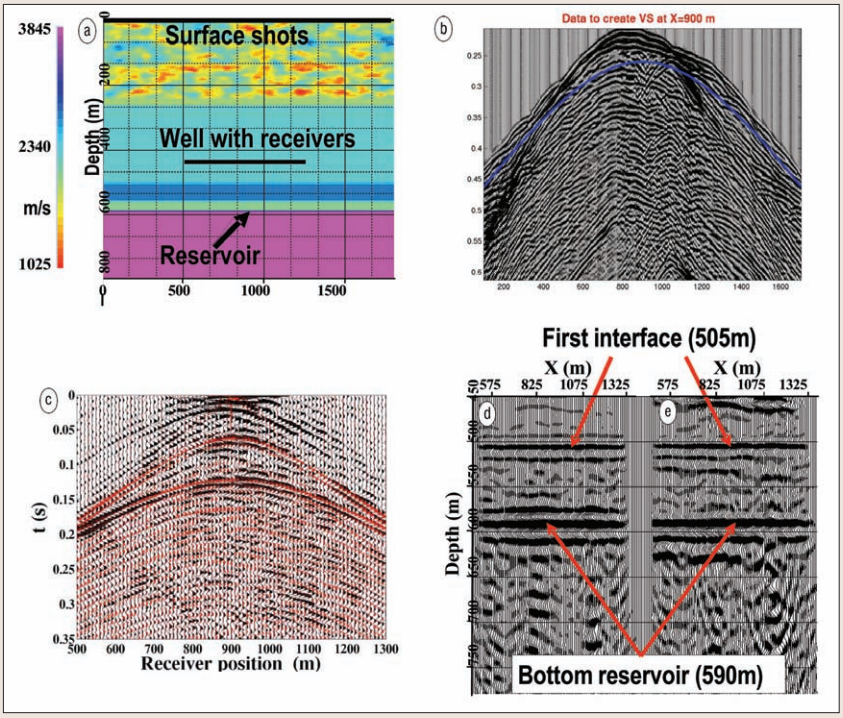

Figure 6. Synthetic Peace River model to image through complex overburden with virtual source technology: (a) P-wave velocity model with very heterogeneous near-surface layer; (b) common-receiver gather showing great distortions of the VSP wavefield; (c) common virtual source gather (red) compared to ground truth response of buried source (black); (d) VS image obtained with 1D velocity model beneath the well; (e) image of VSP data assuming unrealistic scenario where exact near-surface velocity model is known.

Not needing velocity information about the overburden is useful not only in permafrost areas and rugged terrains, but also near the edges of salt, where complex geometries and rapid changes in sediment velocity and anisotropy are difficult to model and leave imprints on the target images below. Even if such model inaccuracies could be overcome, the complicated scattering from strong heterogeneities in the overburden becomes noise that degrades the images in conventional processing. In contrast, overlying model errors are irrelevant for virtual source synthesis and complex scattering can be a beneficial fuel for the virtual source wavefield. Indeed, scattered high frequencies that get stacked out in conventional processing are not lost in the virtual source creation, and therefore, are available for high-resolution imaging of the medium below the virtual source locations.

To image with virtual sources we need velocity information for the relatively small region between them and the target. This velocity can be estimated from sonic logs or virtual check shots and, even if uncertain, it can lead to useful images because the target is relatively close. This idea has been exploited in the literature for imaging salt flanks with real and synthetic data and is being explored by Shell operating units for subsalt imaging (Figure 7).

With suitable acquisition, one may image salt flank recumbencies, which are very difficult to define from surface seismic data. The key to success is presurvey modeling, as physical sources need to be far from the well bore, and a complex 3D salt flank may not be amenable to this type of 2D imaging.

Salt cavern modeling study. One may also image salt flanks from within salt. This novel idea is being tested in a salt dome in The Netherlands, where a Shell operating unit is assisting the salt mining company Akzo Nobel in the evacuation of salt caverns for underground gas storage by the Dutch gas companies Gassunie and NUON. The caverns will be 300 m in height with a diameter of 60 m, starting at depths of 1 km. They must be at least 100 m from the salt flank (Figure 8). The Zuidwending salt dome is an upward lobe of the Zechstein salt formation, which tightly seals the huge, underlying Groningen gas field. The geometry of the salt dome has been derived from surface seismic, but it remains rather uncertain (+/- 200 m) along the vertical flanks (Figure 8). A salt proximity survey would require very distant sources to image a useful portion of the salt flank, and would be very uncertain. On the other hand, generating virtual sources in the salt, we could image the salt flank needing only the salt velocity for accurate lateral positioning.

The acquisition will be a conventional walkaway VSP with receivers in the salt cavern pilot holes. Shot locations were initially chosen based on ray tracing to image the desired portion of the salt flank (Figure 9, top). We also generated a full waveform 2D elastic synthetic data set with a free surface. The salt flank reflection is discernible on the raw common receiver gathers but is obscured by top salt multiples. After application of virtual source technology, the salt flank reflection becomes clean and easy to pick, especially on the zero-offset gather (Figure 9, bottom). Picking the times on the synthetic data we reproduced the model interface with better than 25-m precision, which was sufficient to justify acquisition.

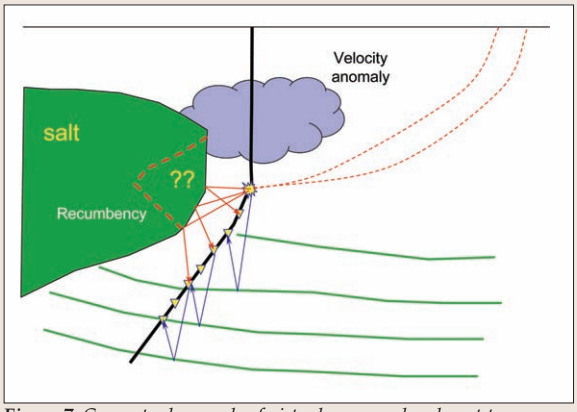

Figure 7. Conceptual example of virtual sources placed next to or under salt to image reflectors below without regard to overlying velocity complexities. Illuminating receivers at virtual source locations from the side (dashed raypaths) can resolve possible salt flank recumbencies hard to image from surface.

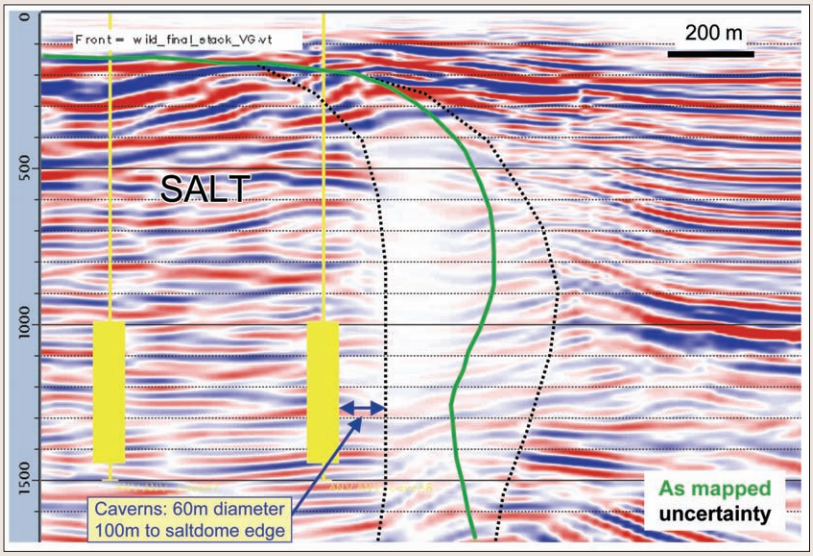

Figure 8. Planned salt caverns for underground gas storage in The Netherlands. Uncertainty of lateral positioning of salt flank from surface seismic needs to be reduced for safe placement of salt cavern.

High-fidelity and in-situ time-lapse seismic. Virtual source monitoring has emerged as a complementary tool to conventional time-lapse seismic to address the following challenges:

- Inability to repeat the acquisition geometry (e.g., source and receiver locations)
- False 4D responses due to seasonal changes in the near surface between time-lapse surveys which can be completely overwhelming in certain areas (e.g., Arctic, Siberia).
- Difficulty in tracking small time-lapse signals under complex near surface (typical for Middle East reservoirs)

Seismovie experiments by CGG have demonstrated that high repeatability can be achieved and very small time-lapse signals observed when sources and receivers are placed at fixed locations beneath the layer subject to seasonal changes. While such in-situ 4D seismic is attractive, it requires both sources and receivers to be permanently buried. In contrast, the virtual source method offers essentially the same advantages but requires that only the receivers be permanently buried. Indeed, it has been demonstrated before that, with permanent receivers in the well, virtual source technology corrects for typical geometry nonrepeatability of surface acquisition. We show next that seasonal changes can also be handled, thus enabling sensitive monitoring of small signals. Such high-fidelity time-lapse seismic technology will be key to the success of the Shell Group's next generation Smart Fields in increasingly complex areas.

To demonstrate the ability of this technique to mitigate near-surface seasonal changes, we use the same Peace River model and VSP acquisition in Figure 6. In the baseline survey the upper 5 m of the near-surface layer are assumed to transition from unfrozen wet soil to frozen conditions; in the

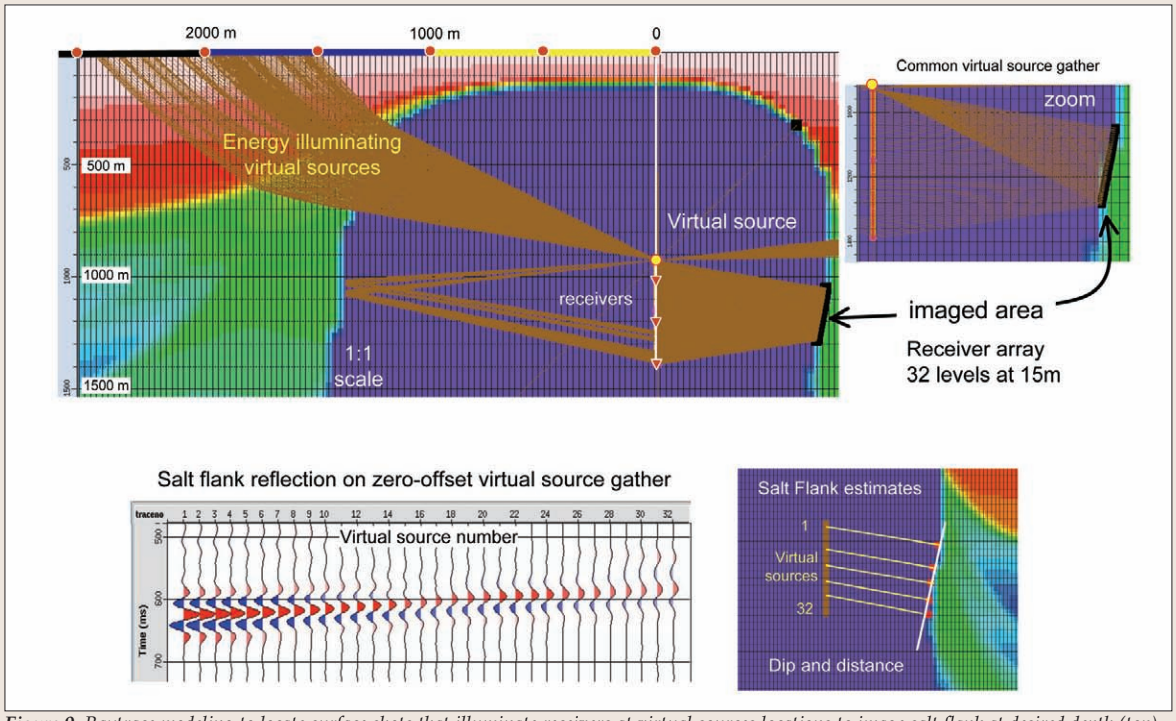

Figure 9. *Raytrace modeling to locate surface shots that illuminate receivers at virtual sources locations to image salt flank at desired depth (top). Zero-offset virtual source traces can be used to estimate distance to salt flank in a simple way (bottom).*

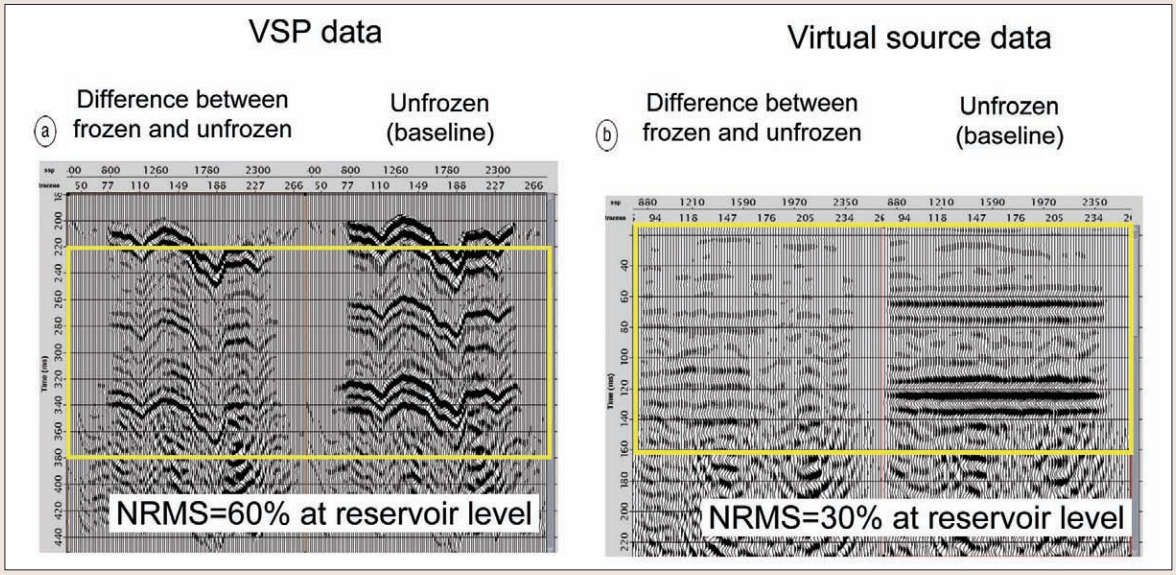

Figure 10. *Modeled images from two surveys recorded under wet (baseline) and frozen (monitor) conditions when no reservoir changes take place. (a) VSP data time-migrated with baseline velocity model. Note strong jiggling of traveltimes due to heterogeneous near-surface and poor repeatability around reservoir zone. (b) VS data time-migrated with 1D velocity model below the well. Note that all time jiggling in the overburden is removed and much better repeatability is achieved without additional acquisition effort.*

repeat survey the entire near surface is assumed frozen. The Voronkov equation

$$\frac{(V_{Pf} - V_{Pw})}{V_{Pf}} = 0.73 - 0.11\, V_{Pw}$$

was used to convert P and S velocities (km/s) of wet soil (V_{Pw}) to corresponding values in frozen soil (V_{Pf}). This very heterogeneous speed-up of up to 100% of the original velocities causes large nonrepeatability even though the reservoir zone remains unchanged. Migrating both baseline and repeat VSP data sets with the same baseline velocity model (wet/frozen) gives a poor repeatability estimate of 60% in

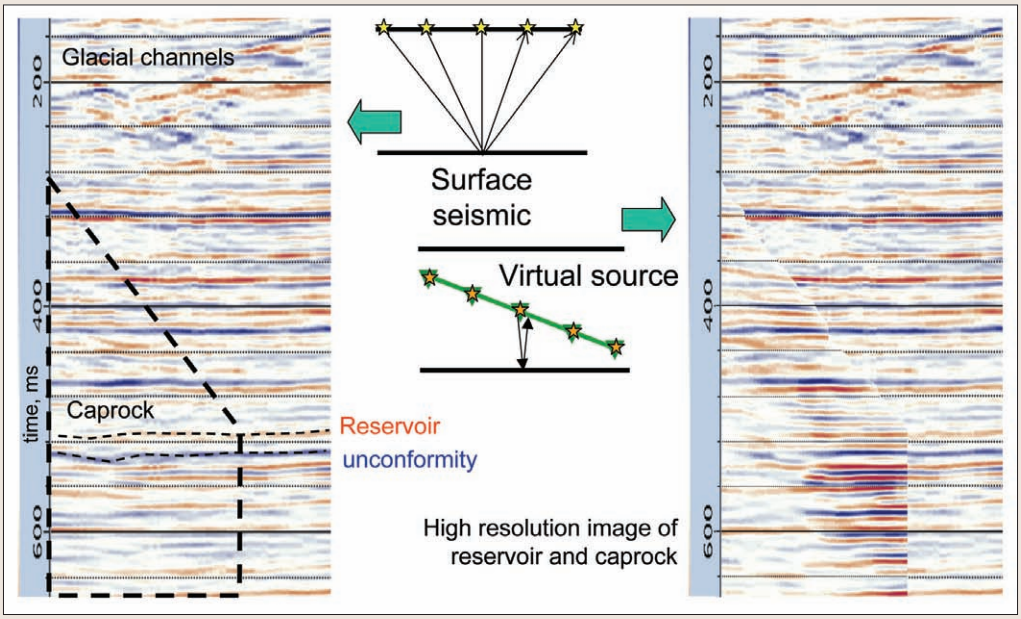

Figure 11. Comparison of surface seismic (left) with zero-offset virtual source image (right) as acquired in a deviated well in Peace River Field in Canada. Application of virtual source technology shows improved resolution of the cap rock and reservoir sections.

normalized rms units and an artifact-ridden baseline image (Figure 10a). In contrast, the corresponding virtual source data give a much improved repeatability estimate of 30% rms and a clear baseline image (Figure 10b). Thus, with application of virtual source technology we have a much better chance of observing production-related time-lapse signals. While our modeled heterogeneities and seasonal velocity changes may be exaggerated, they illustrate the stable performance of this method under conditions unmanageable by other methods.

Our real data example also pertains to Peace River, where massive heavy oil resources are being exploited by cyclic steam stimulation. Studies show that the steam paths in the reservoir are hard to model and must be measured to be able to alter the steam injection patterns to increase recovery from each square-kilometer development pad. Glacial channels overlying the field and seasonal changes in the immediate near surface compromise data quality and repeatability of surface seismic and make us seek downhole solutions with virtual source monitoring. At Pad 40, a well was drilled above the reservoir at an inclination of 45° and instrumented with 50 permanent 3-C geophones. The seismic data sets include a baseline and four repeats of a 2D source line at various stages of the steam injection cycle, with simultaneous surface and downhole recording. We have processed the downhole data to synthesize virtual sources at each receiver location and focused our attention on the upgoing, zero-offset virtual source reflections. This basic single-fold data set ties the corresponding surface seismic and shows increased resolution of the 75-m seal section, the 25-m reservoir, and the unconformity below (Figure 11).

The single-fold virtual source time-lapse images (Figure 12) show very good repeatability above the reservoir and distinct changes in the reservoir and the section below (presumably due to absorption in the heated reservoir). A quantitative evaluation of the changes over time will be attempted, although the results will be of limited use given the small imaged area and an apparent shadow zone near the edge of the survey. Nonetheless, these encouraging results justify a test of areal monitoring, as we discuss below.

Deployment issues and opportunities for monitoring. Monitoring with virtual sources in observation wells is technically feasible with current technology for single instrumented well bores. For field-wide areal monitoring, multiple instrumented well bores are required and several technical and operational challenges need to be overcome.

First, we need to develop inexpensive and reliable methods for drilling horizontal wells in the shallow and deep overburden. A recent U.S. Department of Energy initiative fostered the development of a set of low-cost drilling technologies for vertical, instrumented, very small diameter "microholes." A similar effort seems required for horizontal wells to fully leverage the virtual source method. U-shaped wells (with two surface exits) are particularly attractive for shallow horizontal wells, because they provide great flexibility for sensor deployment.

Second, fit-for-purpose seismic sensor arrays need to become available for this new geophysical market niche. Conventional VSP sensors are designed for very harsh pressure and temperature conditions, and provide good borehole coupling. Their specs are well above those needed for shallow overburden wells, and their cost is not attractive for permanent deployment. Typical surface seismic arrays may have the right specs but are not suitable for deployment in horizontal wells. OBC cables may be the easiest to adapt to borehole conditions, and the presence of a hydrophone sensor would allow routine application of dual-sensor (vertical geophone + hydrophone) wavefield separation for improvement of the virtual source data. Alternatively, repackaging of surface seismic arrays (a la OBC) may allow them to adapt to borehole coupling conditions. Long sensor arrays would also require digital recording and transmission systems.

Third, conveyance methods need to be developed to deploy long seismic arrays in horizontal or deviated wells. While some methods exist and are practiced for wireline VSP and crosswell seismic, the jury is still out on the most effective way of emplacing long arrays with well-coupled permanent sensors in such wells.

For areal monitoring we require repeated application of

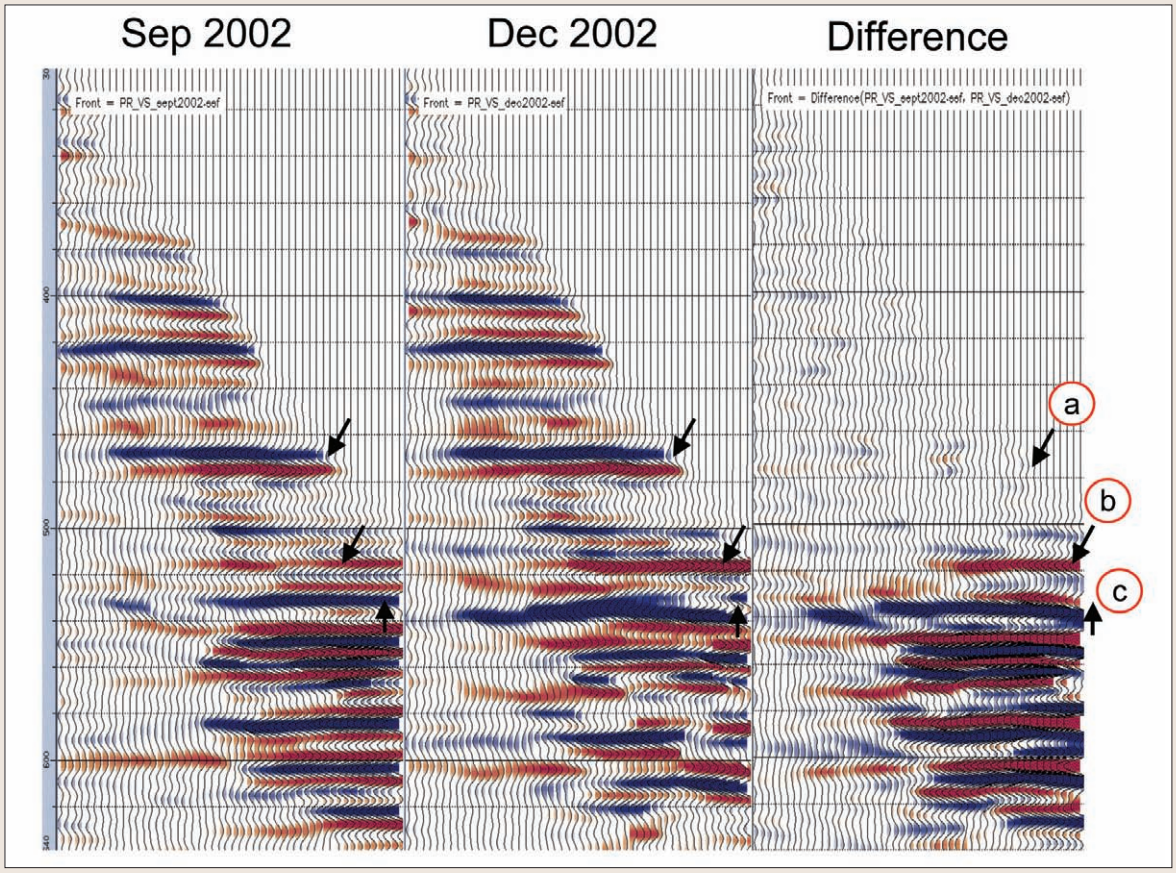

Figure 12. *Zero-offset virtual source image for the baseline (September 2002) and monitor survey (December 2002) after steam injection at Peace River. The arrows on the time-lapse changes on the zero-offset virtual source data point to characteristic events—top seal (a), reservoir (b), and underlying regional unconformity (c). Note the very good repeatability above the reservoir and the marked changes in and below the reservoir.*

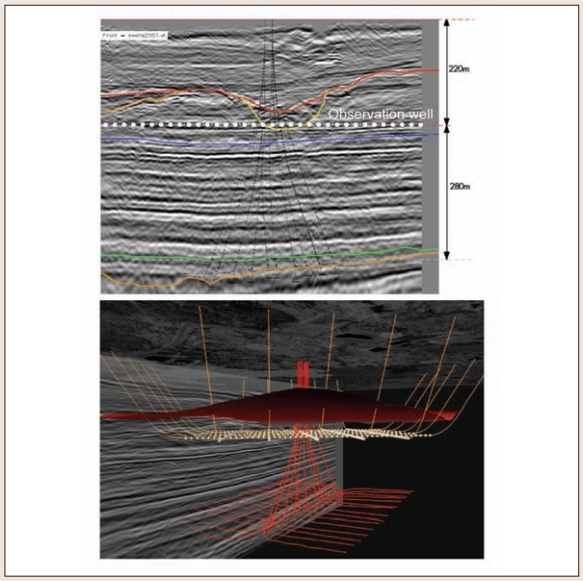

Figure 13. *Conceptual design for areal field monitoring with a grid of instrumented observation wells drilled immediately below the shallow glacial channels at Peace River.*

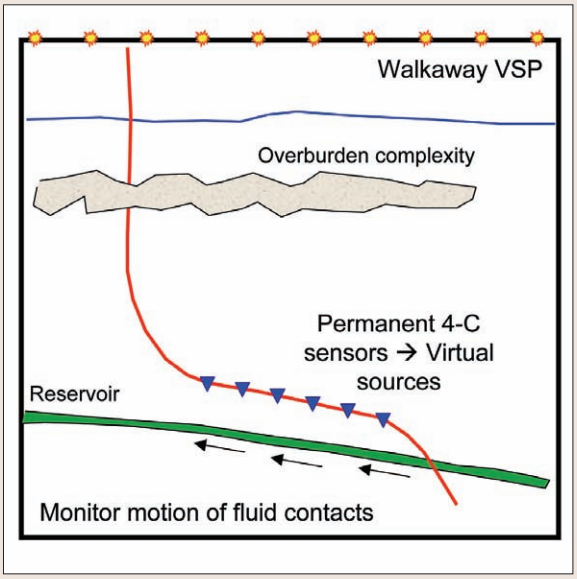

Figure 14. *Conceptual design to monitor a fluid contact with a permanent sensor installation in an injector well.*

these technologies. The simplest configuration is a virtual cross-spread, where an orthogonal pair of instrumented wells is illuminated by an areal surface acquisition, to simulate a buried cross-spread in the subsurface. Field-wide monitoring requires a grid of horizontal wells to image the reservoir with overlapping cross-spreads—e.g., a grid of 5+5 wells to monitor the square-kilometer pads at Peace River (Figure 13). This eventual goal requires the advances in drilling and instrumentation discussed above, although field trials over small areas are being planned for the near future. Besides the operational issues, a challenge remains on the processing of such sparse and possibly irregular data sets.

One may also consider placing permanent sensors in production or injection wells, which by their nature could be highly deviated, for instance when surface obstructions require drilling of extended reach wells from a few drilling centers. A particularly favorable example would be a water injector that has a nearly horizontal section over and along the reservoir from the original fluid contact up to the crest of the structure (Figure 14). If this well section is permanently instrumented and acquired periodically (by shooting a walkaway VSP line over the sensor array), one could monitor the progress of the OWC as the field depletes.

Summary and outlook. Virtual source technology has the potential to revolutionize the ability to probe, image, and monitor the subsurface, especially in areas overlain by very complex overburden. The Shell Group is planning and executing small-scale field trials onshore and offshore, while advances in theory, instrumentation, and drilling technology proceed in parallel. Market forces suggest that a convergence of technical feasibility and cost-effective deployment should occur in the not-too-distant future.

Suggested reading. "Virtual source: new method for imaging and 4D below complex overburden" by Bakulin and Calvert (*SEG 2004 Expanded Abstracts*). "The virtual source method: Theory and case study" by Bakulin and Calvert (GEOPHYSICS, 2006). "Virtual shear source makes shear waves with air guns" by Bakulin et al. (GEOPHYSICS, 2007). "Seismic imaging a subsurface formation" by Calvert (US Patent 6 747 915). "Acoustic time-reversal mirrors" by Fink and Prada (*Inverse Problems*, 2001). "Gas storage in salt caverns" by Hoelen et al. (23rd World Gas Conference, 2006). "VSP: Beyond time-to-depth" by Hornby et al. (*TLE*, 2006). "On the fundamentals of the virtual source method" by Korneev and Bakulin (GEOPHYSICS, 2006). "Integrated reservoir surveillance of a heavy oil field in Peace River, Canada" by Maron et al. (*EAGE 2005 Extended Abstracts*). "Reservoir monitoring using permanent sources and vertical receiver antennae: the Cere-la-Ronde case study" by Meunier et al. (*TLE*, 2001). "A theoretical overview of model-based and correlation-based redatuming methods" by Schuster and Zhou (GEOPHYSICS, 2006). "A novel application of time-reversed acoustics: Salt-dome flank imaging using walkaway VSP surveys" by Willis et al. (GEOPHYSICS, 2006). TLE

Acknowledgments: We thank Shell International Exploration & Production Incorporated for permission to publish this paper; Shell Canada, Akzo Nobel, the Mars Asset, and Plains Exploration are thanked for permission to show the various data sets used in this paper. We also thank the following Shell colleagues for their feedback on the ideas discussed in this paper: R. Calvert, J. Sheiman, J. Wieseneck, W. Langin, M. McRae, H. Dijkerman, P. Mcgillivray, H. van der Heijden, K. Maron, M. Bevaart, A. McGinn, M. Costello, and C. Ellis.

Corresponding author: Jorge.j.l.lopez@shell.com

From order to disorder: a philosophical view on seismic interferometry

Kees Wapenaar, Delft University of Technology, and Roel Snieder, Colorado School of Mines*

Summary

We discuss the phenomenon of 'turning noise into signal' (one of the main properties of seismic interferometry) in the light of changing worldviews, starting with the ordered view of the nineteenth century, via the chaotic world of the twentieth century, to the present view, in which the chaos is tamed.

Introduction

It is by now well-known in ultrasonics (Weaver and Lobkis, 2001), geophysics (Campillo and Paul, 2003; Draganov *et al*., 2007) and underwater acoustics (Roux *et al*. 2004) that the cross-correlation of diffuse wave fields recorded by two different receivers yields the response at one of the receiver positions as if there were a source at the other. This phenomenon is often named 'Green's function retrieval by cross-correlation', whereas in the seismic literature the term 'seismic interferometry' is commonly used (after Schuster, 2004). Although seismic interferometry can be applied to noise as well as controlled source data (see also the 2006 July/August issue of Geophysics), in this paper we only consider its aspect of turning noise into signal. In the present age of chaos theory, one of the most striking properties of seismic interferometry is its robustness. We discuss the phenomenon of 'turning noise into signal' in the light of changing worldviews, starting with the ordered view of the nineteenth century, via the chaotic world of the twentieth century, to the present view, in which the chaos is tamed.

Worldview of the nineteenth century

In the 19th century, the world of physics was one of order. Laplace was a key proponent of the view that the physical world is a deterministic clockwork universe. In this model, the future is completely predictable if one knows the forces between all particles as well as their positions and velocities at any one moment in time. Take, for instance, a soccer player who kicks a ball into a forest (Figure 1). The soccer ball bounces repeatedly off the tree trunks, but if you know the original position of the ball, its velocity and the locations of the trees, the future motion of the ball is determined by the player's initial kick.

Twentieth century physics

With the advent of quantum mechanics in the 20th century, the dream of the universe as a deterministic machine was shattered. Heisenberg's uncertainty principle was the end of the worldview of Laplace: in the quantum world, only the

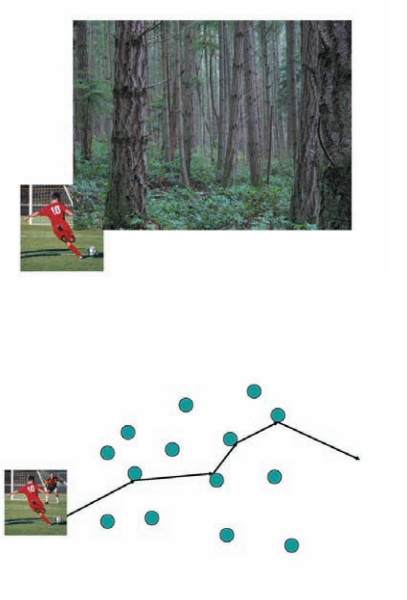

Figure 1. Laplace: the motion of the soccer ball is fully determined by the positions of the trees and the kick of the soccer player.

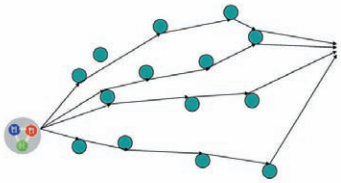

Figure 2. Heisenberg: for an atom-sized soccer ball only the probability of every imaginable trajectory is determined.

probabilities for events are determined by the laws of quantum mechanics. So if an atom-sized soccer ball is kicked into the forest, the trajectory is not determined, but the probability for every imaginable trajectory is (Figure 2). Even for macroscopic systems, determinism did not survive into the 20th century. At that point Poincaré, in a visionary anticipation of chaos theory, showed that even the tiniest uncertainty in the initial conditions can grow exponentially

Reprinted from 77th Annual International Meeting, SEG, Expanded Abstracts, 2683–2687.

DOI:10.1190/1.9781560801924.ch2

From order to disorder to order

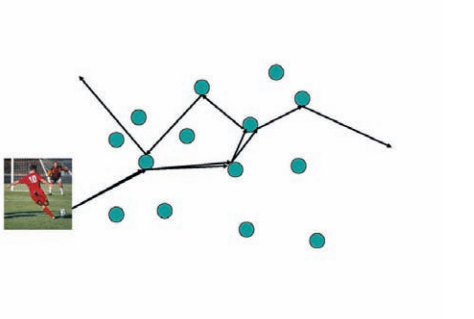

Figure 3. Poincaré: tiny differences in the initial conditions lead to large differences at later times.

with time to make the motion at a later time undetermined, for all practical purposes. So, when the soccer ball is kicked a number of times in slightly different directions, it hits the same trees during the first few bounces at slightly different positions; but the trajectories diverge over time, and after a few bounces the ball may move in completely different ways between the trees (Figure 3).

Particle scattering versus wave scattering

So much for particles: waves behave completely different. If a referee blows his whistle in the same forest repeatedly at slightly different positions, the sound waves scattering between the trees change far less than the motion of the ball (Figure 4). One reason is that waves have an intrinsic length scale, the wavelength, and any perturbations affecting the waves over this are effectively smoothed out. Snieder and Scales (1998) analyzed this mathematically. They showed for a specific configuration with random scatterers that particle scattering becomes chaotic after 8 scatterers whereas wave scattering is still stable after 30 and more scatterers.

Turning noise into signal

Let us now apply the forest analogy to seismic interferometry and see how noise is turned into signal. Imagine it's raining in the forest: every raindrop excites acoustic waves that bounce among the trees in an apparently random fashion. Nevertheless, the trees leave an imprint on the wave field that is characteristic for the forest, just as a fingerprint identifies its owner. The unraveling of this imprint turns out to be surprisingly simple. Let's say there are two microphones in the forest, one of them replacing the whistle-blowing referee (Figure 5). With cross-correlation, we can reconstruct the whistle's sound from the recorded noise of falling raindrops. Take one raindrop that falls in line with the two microphones. The sound wave it generates travels forward, reaching the

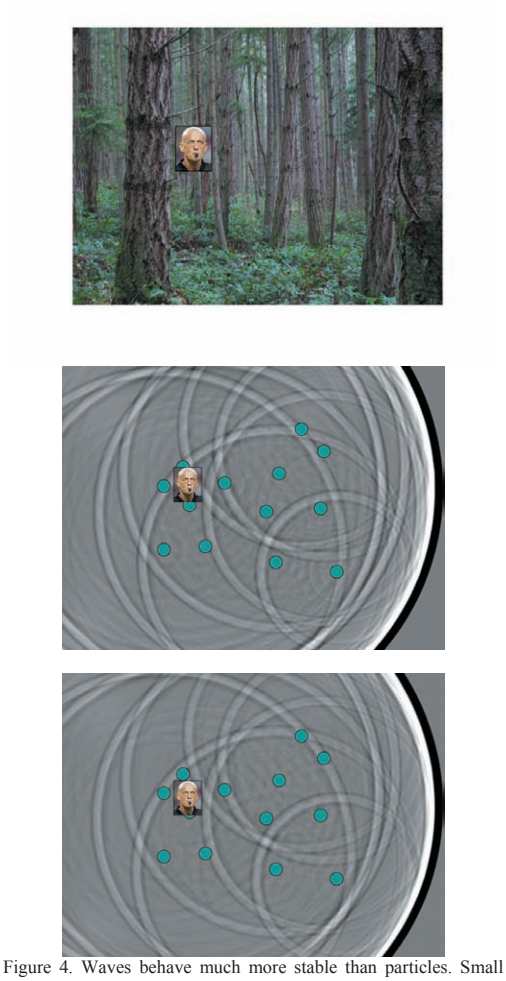

Figure 4. Waves behave much more stable than particles. Small changes in the initial conditions (here: different positions of the referee) are smoothed out at later times.

nearest microphone first and then continuing to the farther one. The difference in the time it takes for the wave to reach each microphone equals the time it takes for the wave to travel between the two microphones. The cross-correlation of the sound waves recorded by the microphones produces a signal at precisely this travel time. So it is as if the first microphone acts as a source, transmitting a weak sound wave to the second. This is enhanced by other raindrops falling in line with the microphones; the rest of the raindrops do not produce a coherent signal. Taking all the coherent waves together, the

From order to disorder to order

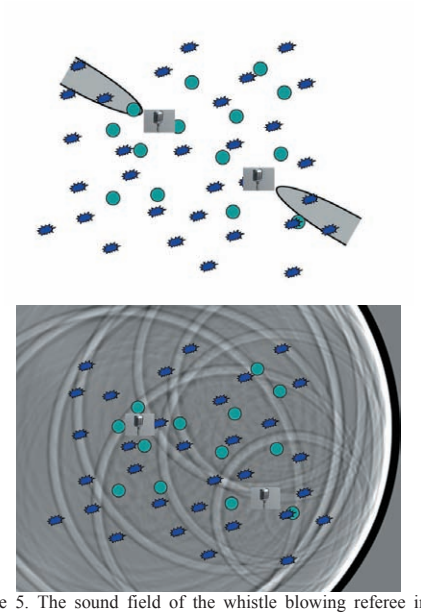

Figure 5. The sound field of the whistle blowing referee in the forest can be reconstructed from the noise of randomly falling raindrops. The raindrops falling in the shaded zones (top frame) contribute to the reconstruction of the direct wave. All scattered waves are reconstructed as well (bottom frame).

first microphone acts as if it is transmitting the sound of the whistle to the second. Mathematics shows that not only the direct wave, but the full wave field (i.e., the full Green's function, including all scattering between the trees), is reconstructed by cross-correlating the wave fields of the raindrops, observed by the two microphones. If this is repeated for multiple microphone positions, the reproduced sound field can be used for imaging – say, to determine the position of nearby trees. This principle creates the opportunity to do wave experiments without using active sources.

Extracting the deterministic response of a system from noise is amazing enough, but there is more. According to theory, noise sources must be distributed homogeneously throughout space, and be uncorrelated – that is, the raindrops must fall everywhere in the forest, and fall at statistically independent times and locations. Astonishingly, in many applications the extraction of the system response from noise has been shown to be fairly robust when noise sources are limited and irregularly distributed, probably because of the stability of wave propagation. Look again at Figure 5 (top frame). Due to the finite wavelength, the raindrops do not need to fall exactly in line with the microphones to produce a coherent signal; all raindrops falling in the shaded areas contribute to the reconstruction of the direct wave of the whistle blowing referee. A similar type of reasoning holds for the reconstruction of the scattered waves.

Fluctuation-dissipation theorem

It has been known since Einstein's seminal 1905 paper on Brownian motion that the diffusion of a particle is related to the way it slows down after it is disturbed in some way, say by a kick. This principle was later generalized to the fluctuation-dissipation theorem, which states that for systems in thermal equilibrium, the deterministic response of the system is related to thermal fluctuations (Callen and Welton, 1951; Le Bellac *et al.*, 2004, see also Figure 6). The research on Green's function retrieval has shown that this principle can be extended to systems so large that thermal fluctuations are irrelevant, such as the sound waves generated by raindrops falling in the forest.

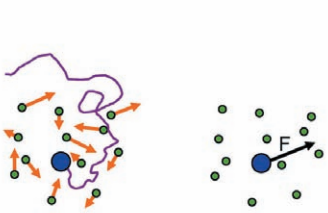

Figure 6. The fluctuations of a pollen particle in a fluid due to the Brownian motion of the fluid molecules are related to the friction forces acting on the same particle, when dragged through the fluid.

Unified Green's function retrieval by cross-correlation

Until recent it was commonly assumed that Green's function retrieval by cross-correlation only works for waves in lossless non-moving media, obeying a wave equation that is invariant for time-reversal. Recent research has shown that the principle holds for a much wider class of systems, where time-reversal invariance does not hold [as for general scalar diffusion phenomena (Snieder, 2006) electromagnetic waves in conducting media (Slob and Wapenaar, 2007), or acoustic waves in viscous media (Snieder, 2007, Extracting the Green's function of attenuating acoustic media from uncorrelated waves: Journal of the Acoustical Society of America, in press)]. With minor modifications it also works in moving fluids, where source-receiver reciprocity breaks down (Wapenaar, 2006; Godin, 2006).

From order to disorder to order

Snieder *et al*. (2007) investigated Green's function retrieval for systems described by scalar equations with arbitrary order time derivatives (note that – in case of real-valued coefficients – time-reversal invariance only holds for even order time derivatives and that this order is 2 in the acoustic wave equation). The general expression for scalar Green's function retrieval contains contributions from sources in a volume and sources on the boundary enclosing the volume. For any lossless system it appears to be sufficient to have sources on the boundary only; for systems with dissipation, sources are required to be present throughout the volume to overcome the dissipation. With these extensions, Green's function retrieval by cross-correlation becomes possible for

- acoustic waves in viscous media,
- electromagnetic waves in conducting media,
- pure diffusion phenomena (with applications in pore fluid pressure propagation in porous media, or diffusive transport of tracers and contaminants),
- Schroedinger's equation (where the 'zero-offset Green's function' is obtained from the intensity fluctuations of the quantum mechanical wave function),
- bending waves in beams (with applications in monitoring bridges, buildings and other mechanical structures, see Figure 7),
- advective transport (with applications for monitoring the temperature in advective heat transport or the concentration of a nonreactive contaminant, see Figure 7), etc.

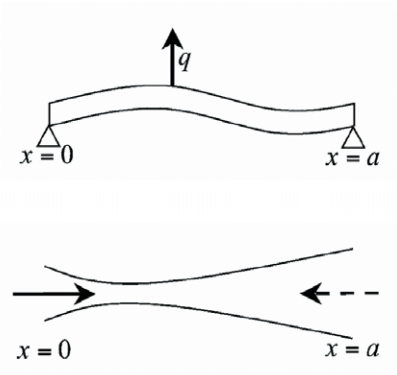

Figure 7: Two of the many new applications of scalar Green's function retrieval by cross-correlation (bending waves and advective transport).

Wapenaar *et al*. (2006) investigated general vector equations and showed that Green's function retrieval by cross-correlation also holds for

- elastodynamic waves in viscous media,
- poroelastic waves in porous media,
- electroseismic waves in porous media (Figure 8),
- electrokinetic waves in piezoelectric media, etc.

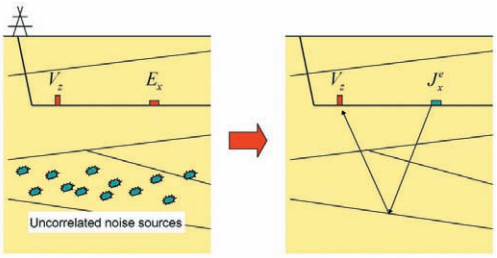

Figure 8: Vectorial Green's function retrieval by cross-correlation: in this example the vertical particle velocity is cross-correlated with the horizontal electric field, yielding the electroseismic response of a horizontal electric current source observed by a vertical geophone.

Conclusions

Our view of the universe may have shifted from the deterministic to the random, but since the turn of the last century physics itself has provided a less simplistic view. Fields generated by random sources can now be used for imaging and for monitoring of systems such as the Earth's subsurface or mechanical structures such as bridges. Randomness is no longer at odds with determinism, but has instead become a new tool providing insights into the deterministic response of the physical world.

EDITED REFERENCES

Note: This reference list is a copy-edited version of the reference list submitted by the author. Reference lists for the 2007 SEG Technical Program Expanded Abstracts have been copy edited so that references provided with the online metadata for each paper will achieve a high degree of linking to cited sources that appear on the Web.

REFERENCES

Callen, H. B., and T. A. Welton, 1951, Irreversibility and generalized noise: Physical Review, 83, 34–40.

Campillo, M., and A. Paul, 2003, Long-range correlations in the diffuse seismic coda: Science, 299, 547–549.

Draganov, D., K. Wapenaar, W. Mulder, J. Singer, and A. Verdel, 2007, Retrieval of reflections from seismic background-noise measurements: Geophysical Research Letters, 34, L04305-1–L04305-4

Godin, O. A., 2006, Recovering the acoustic Green's function from ambient noise cross correlation in an inhomogeneous moving medium: Physical Review Letters, 97, 054301-1–054301-4

Le Bellac, M., F. Mortessagne, and G. G. Batrouni, 2004, Equilibrium and non-equilibrium statistical thermodynamics: Cambridge University Press.

Roux, P., W. A. Kuperman, and NPAL Group, 2004, Extracting coherent wave fronts from acoustic ambient noise in the ocean: Journal of the Acoustical Society of America, 116, 1995–2003.

Schuster, G. T., J. Yu, J. Sheng, and J. Rickett, 2004, Interferometric/daylight seismic imaging: Geophysical Journal International, 157, 838–852.

Slob, E., and K. Wapenaar, 2007, Electromagnetic Green’s functions retrieval by cross-correlation and cross-convolution in media with losses: Geophysical Research Letters, 34, L05307-1–L05307-5.

Snieder, R., 2006, Retrieving the Green's function of the diffusion equation from the response to a random forcing: Physical Review E., 74, 046620-1–046620-4.

Snieder, R. K., and J. A. Scales, 1998, Time-reversed imaging as a diagnostic of wave and particle chaos: Physical Review E., 58, 5668–5675.

Snieder, R., K. Wapenaar, and U. Wegler, 2007, Unified Green's function retrieval by cross-correlation; connection with energy principles: Physical Review E., 75, 036103-1–036103-14.

Wapenaar, K., 2006, Nonreciprocal Green's function retrieval by cross correlation: Journal of the Acoustical Society of America, 120, EL7–EL13.

Wapenaar, K., E. Slob, and R. Snieder, 2006, Unified Green's function retrieval by cross correlation: Physical Review Letters, 97, 234301-1–234301-4.

Wapenaar, K., and R. Snieder, 2007, Chaos tamed: Nature, 447, 643.

Weaver, R. L., and O. I. Lobkis, 2001, Ultrasonics without a source: Thermal fluctuation correlation at MHz frequencies: Physical Review Letters, 87, 134301-1–134301-4.

DOI:10.1190/1.9781560801924.ch2